

Review

# Recent Advances in Supported Metal Catalysts for Syngas Production from Methane

Mohammed Mohamedali, Amr Henni and Hussameldin Ibrahim \* 

Clean Energy Technologies Research Institute (CETRI), Process Systems Engineering, Faculty of Engineering and Applied Science, University of Regina, 3737 Wascana Parkway, Regina, SK S4S 0A2, Canada; mohmohan@uregina.ca (M.M.); amr.henni@uregina.ca (A.H.)

\* Correspondence: hussameldin.ibrahim@uregina.ca; Tel.: +1-306-337-3347

Received: 21 December 2017; Accepted: 2 March 2018; Published: 7 March 2018

**Abstract:** Over the past few years, great attention is paid to syngas production processes from different resources especially from abundant sources, such as methane. This review of the literature is intended for syngas production from methane through the dry reforming (DRM) and the steam reforming of methane (SRM). The catalyst development for DRM and SRM represents the key factor to realize a commercial application through the utilization of more efficient catalytic systems. Due to the enormous amount of published literature in this field, the current work is mainly dedicated to the most recent achievements in the metal-oxide catalyst development for DRM and SRM in the past five years. Ni-based supported catalysts are considered the most widely used catalysts for DRM and SRM, which are commercially available; hence, this review has focused on the recent advancements achieved in Ni catalysts with special focus on the various attempts to address the catalyst deactivation challenge in both DRM and SRM applications. Furthermore, other catalytic systems, including Co-based catalysts, noble metals (Pt, Rh, Ru, and Ir), and bimetallic systems have been included in this literature review to understand the observed improvements in the catalytic activities and coke suppression property of these catalysts.

**Keywords:** syngas production; dry reforming; steam reforming; methane; bimetallic catalyst

## 1. Introduction

The continuous reliance on fossil fuels as a major energy source has a huge influence on the environment contributing in the undesirable increased emissions of anthropogenic greenhouse gases. This growing energy demand is projected to further increase in the future as reported in the 2016 energy outlook by the international energy agency (IEA). With the depletion of the fossil fuel resources, a significant need arises for utilizing the abundant sustainable resources toward producing efficient fuels and chemicals. Furthermore, all of the hydrocarbon fossil fuel based energy sources are nonrenewable in nature; therefore, it is crucial to find efficient ways to deploy these materials in a more sustainable and environmentally benign way. Synthesis gas (syngas), which is a mixture of hydrogen ( $H_2$ ) and carbon monoxide (CO), provides a viable solution as an energy carrier, feedstock for producing hydrogen fuel, and higher value chemicals. Syngas production has a significant contribution in reducing greenhouse gases emission particularly carbon dioxide ( $CO_2$ ) via the more efficient syngas-based power generation plants, as well as fuel cell technologies. Moreover, syngas conversion into clean liquid fuels through the Fischer-Tropsch (F-T) synthesis provides a cleaner route for exploiting fossil fuels by reducing the greenhouse gases emissions at the end-user side. Syngas could be produced from various feedstocks including gaseous, solid, and liquid hydrocarbons using processes, such as dry reforming (DR), steam reforming (SR), partial oxidation (POX), and autothermal reforming (ATR). The aforementioned processes differ in the amount of heat required and the product

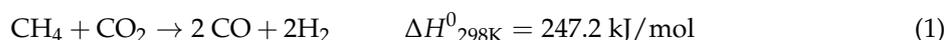
distribution, which is mainly dependent on the nature of the feedstock that is used and the operating conditions [1]. For instance, hydrogen fuel is mostly produced from the steam reforming processes of natural gas and other oxygenated hydrocarbons due to the high concentration of hydrogen in the produced syngas. On the other hand, the gasification of solid hydrocarbons mainly produces syngas that could be consumed directly as a fuel in power plants and internal combustion engines [2]. A detailed comparison analysis of the advantages and disadvantages between the different syngas production processes is reported by Wilhelm and coworkers to determine the optimum combination of processes for the production of syngas to be used in Fischer-Tropsch (F-T) synthesis [3]. A similar study has been conducted to investigate the different scenarios for syngas production based on the required scale of the production and the target application [4]. The use of catalysts in DRM and SRM reactions is essential to improve the reaction kinetics and achieve a maximum production of syngas by reducing the activation energy of the desired reactions without being consumed in the process. Moreover, since both DRM and SRM reactions are endothermic processes, the presence of a catalyst significantly helps to reduce the necessary temperature to obtain the products. Nevertheless, in all of the processes that are used for syngas production the role of the catalyst used is detrimental to the overall conversion, H<sub>2</sub>/CO ratio, and the energy requirement of the process. Several attempts have been made to develop catalytic systems with improved resilience to coke formation, as well as using cheaper precursors. These includes, the variation of synthesis methods, synthesis conditions, using mixed support approach, and bimetallic systems [5]. The current work provides a summary of the state of the art in the field of metal-oxide catalysts used in the different processes for syngas production with special focus on syngas production from methane using dry and steam reforming processes. The recent advancement that was achieved in the past five years in the fields of metal-oxide catalysts synthesis, characterizations, and performances in syngas production are thoroughly reviewed. A great attention is paid to address the issues that are related to catalyst deactivation during syngas production processes.

## 2. Syngas Production from Methane

Gaseous hydrocarbons, such as methane (CH<sub>4</sub>), are considered to be the major feedstock that is used for syngas production through various technologies and processes to meet the requirement of fuel cell applications, gas to liquid conversions, and chemical production. Methane is considered to be the primary constituent of natural gas that is available in abundant quantities from oil and gas reserves as well as landfill gas [6], and could be envisaged as a potential and reliable feedstock for clean fuels and chemical synthesis. Other sources of methane include biogas, which is produced from the decomposition of organic compounds in the environment. The direct emission of CH<sub>4</sub> into the atmosphere contributes to about 20% of the global warming second to CO<sub>2</sub> contribution; therefore, developing technologies for the conversion of CH<sub>4</sub> into higher value products is substantially essential. The two major processes considered in this work for the production of syngas from CH<sub>4</sub> are the dry reforming of methane (DRM), and the steam reforming of methane (SRM). In the following sections, the catalysts used in the various processes for the conversion of methane into syngas are comprehensively reviewed.

### 2.1. Dry Reforming of Methane (DRM)

The DRM reaction utilizes two significant greenhouse gases (CH<sub>4</sub> and CO<sub>2</sub>) to produce a cleaner form of energy carrier (i.e., syngas) that could be transformed into hydrogen fuel or valuable chemicals [5].



From Reaction (1) the produced syngas has H<sub>2</sub>/CO ratio equal to 1:1, which is well suited for the synthesis of oxygenated hydrocarbons, and F-T synthesis.

The development of efficient catalysts for DRM is essential to achieve high syngas production, while maintaining a longer lifetime for the catalyst. The common metals used for DRM are transition metals (Ni, Co, and Cu), as well as noble metal catalysts (Rh, Ru, and Pt) supported on oxide-based materials. Theoretical calculations have proven the superior performance of noble metal catalysts in terms of having higher catalytic activity and resistance to deactivation, however, they are considered expensive for commercial use. On the other hand, transition metals, particularly Ni based catalysts, are relatively cheaper and have good catalytic properties with the major drawback being prone to deactivation due to coke formation, especially at high temperatures [5]. Table 1 summarizes the recent advances in the application of Ni based catalysts for DRM along with the CH<sub>4</sub> conversion values reported at different temperatures. In the following sections we will discuss in details the various strategies adopted to improve the catalytic performance of Ni-based systems in DRM.

### 2.1.1. Effects of the Support on the Catalytic Activity in DRM

A typical metal-oxide catalyst is composed of active metal sites and a support surface to provide the necessary surface area for the dispersion of metals [7]. The attributes that are required in a promising support material include the high surface area, thermal and chemical stability, high oxygen storage capacity, and the support basic-acid characteristics. Moreover, the support material contributes in the DRM reaction through the metal-support interaction, which plays a vital role in the overall catalytic activity and stability. Al<sub>2</sub>O<sub>3</sub>, which is available commercially, is considered to be the main support material used for DRM with Ni-based catalysts [5]. Wenlong and coworkers have recently studied the preparation of Al<sub>2</sub>O<sub>3</sub> support and reported a comparison with commercial  $\gamma$ -Al<sub>2</sub>O<sub>3</sub> [8]. The catalytic activity evaluation was conducted in a fixed bed reactor using reaction temperature = 800 °C, reaction pressure = 1 atm, CH<sub>4</sub>/CO<sub>2</sub> = 1 (V/V), and gas hourly space velocity (GHSV) = 14,400 mL/(gcat·h). The authors have concluded that the template synthesis approach produces Al<sub>2</sub>O<sub>3</sub> support with higher surface areas and basicity than the commercial counterpart and therefore exhibited enhanced CH<sub>4</sub> conversion and could be considered for practical application. Modifications of the support basicity was also recently investigated using phosphorous (P) as a modifier in Ni/Al<sub>2</sub>O<sub>3</sub> catalyst [9]. The findings of this study have confirmed the proportional correlation between the support surface basicity and its catalytic activity due to the induced acid-base interaction between the basic support and the acidic CO<sub>2</sub> leading to the dissociation of CO<sub>2</sub> during DRM. The 10 wt % Ni/Al<sub>2</sub>O<sub>3</sub> catalyst with 2 wt % P exhibited the highest stability with an activity loss of 7% over 100-h reaction period when compared to 32% for the unmodified 10 wt % Ni/Al<sub>2</sub>O<sub>3</sub>. Das et al. have argued that increasing the support basicity is not absolutely beneficial to improve the catalytic activity in DRM but it is rather preferred to have a moderate acid to base ratio in the catalyst [10]. The argument was justified by the fact that the acidic CO<sub>2</sub> will preferentially adsorb on the basic sites while methane decomposition will proceed on the acidic sites; hence the control of acid/base ratio is essential to obtain optimum activation energies of the two reactions (CO<sub>2</sub> disproportionation and CH<sub>4</sub> decomposition). To systematically investigate the impact of the acid/base ratio in DRM reaction, modified silica and alumina supports have been synthesized using a single and two-step synthesis methods. Figure 1 demonstrate the argument that is made by Das et al. that at higher acid/base ratio, methane decomposition was more favored (lower activation energy for CH<sub>4</sub>), while at lower acid/base ratios (higher basicity), the activation of CO<sub>2</sub> through Boudouard reaction and metal oxidation was predominant. On the other hand a moderate acid/base ratio (around 1.7) displayed the highest TOF (Figure 1a), which could be attributed to the comparable rates of CH<sub>4</sub> cracking and CO<sub>2</sub> splitting, which releases enough oxygen to immediately remove the deposited carbon.

Although alumina has shown a superior catalytic activity as a support in DRM, it has a major challenge, which is phase transformation into alpha phase alumina ( $\alpha$ -Al<sub>2</sub>O<sub>3</sub>), which has propelled the search for other potential support materials. Rong-jun et al. has presented a comparison between different support materials (SiO<sub>2</sub>, TiO<sub>2</sub>, ZrO<sub>2</sub>, MgO, and Al<sub>2</sub>O<sub>3</sub>) that are impregnated with a Ni loading of 8 wt % in DRM [11]. SiO<sub>2</sub> has shown the highest surface area as compared to the other

support materials, however it has a low interaction with the metal sites, leading to low dispersion and easily reducible catalysts, which is not favorable for DRM reactions. All of the supports excepts for  $\text{Al}_2\text{O}_3$  and  $\text{MgO}$  has displayed a low reduction temperature between 300–500 °C, while  $\text{Al}_2\text{O}_3$  was stable beyond 600 °C, which could be ascribed to the formation of  $\text{NiAl}_2\text{O}_4$  spinel, indicating a strong interaction between  $\text{NiO}$  and  $\text{Al}_2\text{O}_3$  as was evident from the  $\text{H}_2$  temperature programmed reduction ( $\text{H}_2$ -TPR) profiles similar to previous observations [12].  $\text{MgO}$  support has a wide range of reduction temperature, which starts at 200 °C until 950 °C, which could be attributed to the formation of  $\text{NiO-MgO}$  solid solution. The strong basic centers on  $\text{MgO}$  acts as active sorption sites for  $\text{CO}_2$  during the DRM reaction, which consequently suppress the hydrogenation reaction of  $\text{CO}_2$  toward coke formation and hence improves the catalyst stability [13]. Therefore, the authors have also impregnated  $\text{Ni}$  metals on  $\text{MgO-Al}_2\text{O}_3$  support to benefit from the synergism between the two individual materials. The deployment of the mixed support has resulted in a significant improvement in both the  $\text{CH}_4$  conversion and most importantly the coke deposition rate which was reported to be the lowest amongst the studied supports mainly due to the strong interaction between  $\text{NiO}$  and  $\text{Al}_2\text{O}_3$  and  $\text{MgO}$ , as indicated by the small particle size and large specific surface area of the metal sites. These observations were supported by a recent study for the impregnation of different  $\text{Ni}$  loadings on  $\text{MgO-Al}_2\text{O}_3$  via the co-precipitation technique [14]. The enhanced catalytic activity and prolonged catalyst lifetime was also attributed to the small particle size and high specific surface area up to a  $\text{Ni}$  content of 15 wt %. The catalyst reduction temperature was reported to be between 800–900 °C regardless of  $\text{Ni}$  loadings, which was higher than the values observed by Rong-jun et al. (600–900 °C) [11]. Furthermore, according to  $\text{N}_2$  adsorption experiments the  $\text{Ni/MgO-Al}_2\text{O}_3$  catalyst prepared by [14] has a mesoporous structure with pore size of 2–9 nm which is smaller than the same catalyst reported by Rong-jun et al. [11]. Nevertheless, it is important to mention that the idea of a direct correlation between the  $\text{MgO}$  content in the catalyst and its acid/base properties have been recently challenged [15]. Although the positive impact of  $\text{MgO}$  on the catalytic activity of  $\text{Ni/ZrO}_2$  in DRM reaction was also realized in the recent study, the correlation of acid/base property to the  $\text{MgO}$  content is not accurate. More investigations are therefore required to understand the relationship between the support constituents, the observed characterizations, and the catalytic performance.

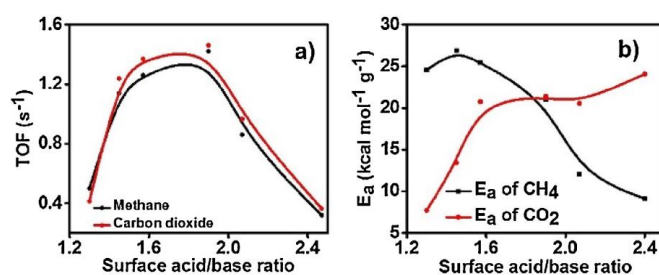


**Figure 1.** Variation of (a) turnover frequency (TOF) with acid/base ratio and (b) activation energy with acid/base ratio. Reproduced with permission from [10].

$\text{CeO}_2$  was reported to have excellent characteristics as a support material for  $\text{Ni}$  impregnation in DRM reactions, owing to its high oxygen mobility and positive impact on the oxidation state of  $\text{Ni}$  species [12,16,17]. However, the beneficial impact of  $\text{CeO}_2$  are more pronounced when used as a promotor for  $\text{Al}_2\text{O}_3$  supports as demonstrated by Haghghi and coworkers [18]. Two different synthesis methods were utilized to prepare the  $\text{Ni/CeO}_2\text{-Al}_2\text{O}_3$  catalyst namely the sol-gel and sequential impregnation approaches. It was concluded that the addition of 10 wt %  $\text{CeO}_2$  as a promotor has reduced the overall surface area, but resulted in a uniform distribution of small particle size  $\text{Ni}$  species, showing higher catalytic activity and stability than the unmodified  $\text{Ni/Al}_2\text{O}_3$  up to 10 h at 850 °C. The catalytic DRM experiments were carried out at atmospheric pressure in the temperature range of 550–850 °C with feed ratio of  $\text{CH}_4/\text{CO}_2 = 1$ . Both syntheses approaches has shown a stable performance up to 10 h however,

sol-gel synthesis technique recorded a considerably higher  $\text{CH}_4$  conversion than the impregnation route (90% versus 35% at 750 °C). In a similar study by Han et al. [19], the addition of 2 wt %  $\text{CeO}_2$  to  $\text{Al}_2\text{O}_3$  was studied at different Ni loadings (5–30 mol %) to get insights into the carbon resistance ability of  $\text{CeO}_2$ -modified catalysts. The stability test was carried out on 10 wt % Ni/ $\text{CeO}_2$ - $\text{Al}_2\text{O}_3$  catalysts at 750 °C for 30 h with a GHSV of 40,000 mL  $\text{g}^{-1} \text{h}^{-1}$ . Under these conditions, the formation of carbon nanotubes was confirmed from scanning electron microscopy (SEM) scans, however it was believed that it has no impact on the stability, and hence, the improved stability of  $\text{CeO}_2$  was attributed to the suppression of graphite-like carbons confirming previous findings for  $\text{CeO}_2$ -modified  $\text{SiO}_2$  [20] and  $\text{CeO}_2$  modified  $\text{MgO-Al}_2\text{O}_3$  [21]. To further understand these observations, in-situ XRD and  $\text{H}_2$ -TPR were conducted to gain more insights into the structural evolution of the catalyst and correlate the  $\text{CeO}_2$ - $\text{Al}_2\text{O}_3$  mixed oxide catalyst with the catalytic performance. The XRD diffraction patterns of the 10 wt % Ni/ $\text{CeO}_2$ - $\text{Al}_2\text{O}_3$  catalyst is shown in Figure 2. It can be clearly observed that the calcined catalyst at room temperature, characteristic peaks were detected for  $\text{CeO}_2$  (28.5°, 33°, 47.5°, and 56.3°), NiO (44.5°, 51.9°, and 76.4°), and  $\text{NiAl}_2\text{O}_4$  spinel (37°, 44.9°, 59.6° and 65.5°). However, at a reduction temperature of 750 °C these peaks showed lower intensities and moved to lower angles indicating the complete reduction of  $\text{Ce}^{4+}$  and  $\text{Ni}^{2+}$ , while new peaks for Ni phase has appeared. These observations were confirmed by the  $\text{H}_2$ -TPR results (not shown here) which shown a reduction of NiO to  $\text{Ni}^0$  (a small band at 250–400 °C) and the formation of  $\text{CeAlO}_3$  (a main peak at 825 °C). In a similar study, Munoz et al. [22] reported the incorporation of Ni into  $\text{CeO}_2$ -YSZ and  $\text{Ce}_{0.15}\text{Zr}_{0.85}\text{O}_2$  supports as catalysts for DRM reaction at 750 °C and atmospheric pressure. The high catalytic activity and stability exhibited by the two catalysts was attributed to the excellent oxidative nature of the support material that induced the oxidation of the carbonaceous materials formed during the DRM reaction. Furthermore, the Ni/ $\text{CeO}_2$ -YSZ catalysts showed superior stability at space velocity of 60,000  $\text{cm}^3/\text{g}/\text{h}$  and undiluted equimolar feed ( $\text{CH}_4:\text{CO}_2 = 1$ ) compared to Ni/ $\text{Ce}_{0.15}\text{Zr}_{0.85}\text{O}_2$ , which lost its stability almost immediately. Several characterization techniques including Raman spectroscopy, Thermogravimetric Analysis (TGA), Transmission Electron Microscopy (TEM), and X-ray Photoelectron Spectroscopy (XPS), were deployed to investigate the nature of the coke deposited on the spent catalysts. Two peaks were observed in the derivative TGA profile, with the low temperature peak corresponding to reactive carbon, whereas the high temperature peak represents a more crystalline coke. The strong Ni-support interaction as observed from the XPS spectra (not shown here) of the spent catalyst was responsible for the catalyst stability through the preservation of the metal dispersion via a kinetically balanced oxidation-carbonation reactions. The prolonged stability for undiluted feed streams was also reported for Ni/CeMgAl catalyst that was prepared using refluxed co-precipitation technique and was also ascribed to the presence of both  $\text{CeO}_2$  and MgO in the support [23].

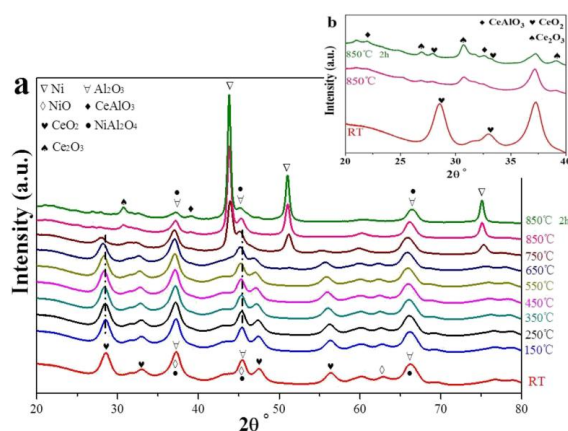


**Figure 2.** In-situ XRD patterns of 10 wt % Ni/ $\text{CeO}_2$ - $\text{Al}_2\text{O}_3$  catalyst (a) reduced from room temperature (RT) to 850 °C and kept at 850 °C for 2 h; (b) from 20° to 40° at RT, 850 °C and after reduction at 850 °C for 2 h. Reproduced with permission from [19].

**Table 1.** Ni-based metal-oxide catalysts for dry reforming of methane (DRM).

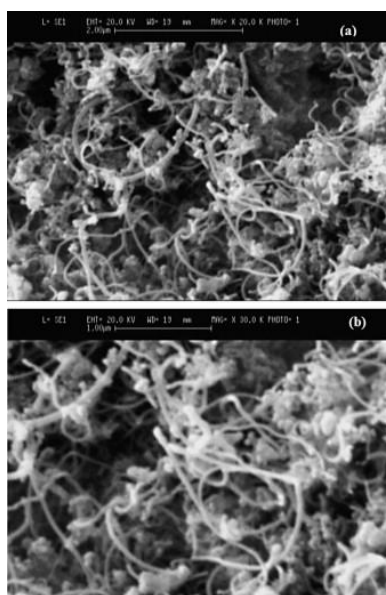
Metal	Support	Temperature (K)	CH <sub>4</sub> Conversion	H <sub>2</sub> /CO	Remarks	Ref.
Ni	Nd-mesoporous silica	973	53	0.75	Mesoporous silica support was modified using Neodymium (Nd) to improve the metal dispersion and support basicity	[24]
Ni	La-ZrO <sub>2</sub>	555	22.8	0.83	The use of electric field to improve the catalytic performance of DRM was studied, and it was concluded that the electric power accelerates the surface reaction of CH <sub>4</sub> hence reaction can proceed at very low temperatures	[25]
	Ce-ZrO <sub>2</sub>	545	13.2	0.75		
	Pr-ZrO <sub>2</sub>	538	15.2	0.78		
	Nd-ZrO <sub>2</sub>	498	12.5	0.88		
	Y-ZrO <sub>2</sub>	496	12.4	0.75		
Ni	Ce-Al	1073	90	1.1	The reflux precipitation synthesis method was used to prepare different Ni loadings on Ce-Al support which achieved improved stability due to the existence of various Ce, Al, and Ce-Al oxides with excellent oxidative properties that burns off the deposited carbon	[19]
Ni	CeO <sub>2</sub>	1073	95	2	Impregnation synthesis was used to prepare the catalyst to be used under chemical looping DRM conditions to achieve high H <sub>2</sub> /CO ratios due to the continuous oxidation-reduction of the catalyst	[17]
Ni	Ce-ZnAl <sub>2</sub> O <sub>4</sub>	1073	82	1	Cerium (Ce) was used as a support promotor using co-precipitation method to improve the Ni dispersion and reduce particle size to achieve longer catalyst lifetime	[26]
Ni	γ-Al <sub>2</sub> O <sub>3</sub>	NA	30	1	Dielectric plasma was used to improve the catalytic performance for DRM and the impacts of the different process conditions (Ni loading, feed composition, and discharge power) was statistically correlated	[27]
Ni	Si microspheres	1023	70	0.8	Sol-gel microencapsulation synthesis was used to prepare the catalyst, and the conversion of the carbon formed into SiC was confirmed which prevented catalyst deactivation	[28]
Ni	Al <sub>2</sub> O <sub>4</sub>	1073	90	0.81	Co-precipitation synthesis was used to prepare catalysts with improved activity and stability attributed to the small crystallite size, high surface area, and the good metal dispersion	[29]
Ni	MgO-Al <sub>2</sub> O <sub>3</sub>	973	74	0.94	The small metal cluster size and high surface areas were deemed responsible for the observe activity and stability.	[14]
Ni	Al <sub>2</sub> O <sub>3</sub> CeO <sub>2</sub> - Al <sub>2</sub> O <sub>3</sub>	1023	70	1	Sequential impregnation versus sol-gel synthesis methods were compared for the preparation of the catalyst. The sol-gel route resulted in a small particle size with enhanced dispersion and catalytic activity	[18]
		1023	90	1		
Ni	γ-Al <sub>2</sub> O <sub>3</sub> CeO <sub>2</sub> -YSZ Ce <sub>0.15</sub> Zr <sub>0.85</sub> O <sub>2</sub>	1023	68	0.75	The excellent catalytic performance of CeO <sub>2</sub> -YSZ as a support for Ni catalyst was ascribed to its high oxidative abilities leading to an increased Ni dispersion and hence reducing carbon deposition	[22]
		1023	100			
		1023	100			
Ni	SBA-15	1023	92	0.98	The optimum operating conditions were developed using SBA-15 with high surface area suitable for high Ni content impregnation	[30]
Ni	MgO-SBA-15	1073	96	1.1	A comparison between the impregnation route versus coating for introducing MgO into the porous structure of SBA-15 was investigated	[13]
Ni	Ce <sub>0.75</sub> Zr <sub>0.25</sub> -SBA-15	1073	100	0.9	The catalyst lifetime was increased by adding CeZr into the SBA-15 support as oxygen providers	[31]
Ni	CaFe <sub>2</sub> O <sub>4</sub>	1073	90.04	0.98	The support was prepared by sol-gel method and the Ni was introduced using wet impregnation technique. Predictions of the DRM was performed using Artificial Neural Network (ANN) based on metal loadings, feed composition, and reaction temperature.	[32]
Ni	SiO <sub>2</sub> (core-shell) SiO <sub>2</sub> (conventional impregnation)	1023	86	0.98	Water in oil micromulsion technique was used to prepare the catalyst with a core-shell structure which reduced Ni sintering during DRM	[33]
		1023	74	0.65		
Ni	ZrO <sub>2</sub>	1123	97	1	Monoclinic ZrO <sub>2</sub> substrates were prepared by adjusting the catalyst synthesis conditions to vary the support surface morphology leading to higher dispersion, surface oxygen availability, and hence showing superior performance to conventional supports	[34]
Ni	ZSM-5	1073	66	0.95	Introducing Co to Ni/ZSM-5 catalyst has significantly improved the catalyst stability due to the activity of Co in oxidation reactions	[35]
Ni	Ce-Zr-SBA-15	873	63	0.85	The effect of Ce-Zr doping into Ni/SBA-15 prepared using different impregnation strategies was studied to gain insights into the role of the synthesis route on the catalyst activity and stability	[36]
Ni	SiO <sub>2</sub> TiO <sub>2</sub> Al <sub>2</sub> O <sub>3</sub> ZrO <sub>2</sub> MgO MgO-AL <sub>2</sub> O <sub>3</sub>	1023	88	0.8	The catalytic performance of different metal-oxides support were tested for DRM and it was concluded that MgO modified Al <sub>2</sub> O <sub>3</sub> possess a great stability due to the improved dispersion and the strong metal-support interaction	[11]
		1023	3			
		1023	78			
		1023	88			
		1023	90			
		1023	87			
Ni	CeMgAl	1073	96.5	0.8	The reflux co-precipitation technique was used to prepare the catalyst and the effects of the calcination and reduction temperatures were evaluated	[23]
Ni	Al <sub>2</sub> O <sub>3</sub> -ZrO <sub>2</sub>	1123	85	0.95	A comparison between catalyst preparation methods was presented	[37]
Ni	Al <sub>2</sub> O <sub>3</sub>	1073	93	1.3	The catalytic performance of Ni supported onto two different supports was investigated	[38]
Ni	CeZrO <sub>2</sub>	1073	91	0.9		
Ni	CeO <sub>2</sub> -SiO <sub>2</sub>	1073	98	1.2	The physicochemical properties of the catalyst were improved by using the mixed oxide approach	[20]

Table 1. Cont.

Metal	Support	Temperature (K)	CH <sub>4</sub> Conversion	H <sub>2</sub> /CO	Remarks	Ref.
Ni	Al <sub>2</sub> O <sub>3</sub>	1073	94	0.86	Different formulations and precursor concentrations were used for the preparation of the Al <sub>2</sub> O <sub>3</sub> support in order to vary the support characteristics and performance in DRM	[8]
Ni	Silicalite	973	65	1.23	The role of the support surface morphology and defects on the catalytic performance in DRM was investigated	[7]
	MCM-41	973	77	1.03		
	Silica delaminated zeolite	973	79	1.39		
Ni	clinoptilolite	1123	88	0.94	The impacts of the support type on the catalyst properties in DRM was analyzed. The utilization of clinoptilolite as cheap support was found promising	[12]
	Al <sub>2</sub> O <sub>3</sub>	1123	93	0.97		
	CeO <sub>2</sub>	1123	75	0.93		

Apart from Ni-based catalysts, numerous studies have been conducted for the development of Co-based metal catalysts for DRM and summarized in Table 2. A recent study by Abasaed and coworkers [39] was conducted for the impregnation of Co into nanosized CeO<sub>2</sub> and ZrO<sub>2</sub> supports calcined at different temperatures. It has been found that the effluent gaseous product for the case of Co/ZrO<sub>2</sub> has higher H<sub>2</sub>/CO ratio than Co/CeO<sub>2</sub> for the same Co content. Moreover, the catalytic activity was favored at lower calcination temperatures due to the observed reduction of surface area when the samples are calcined at higher temperatures (50% reduction in BET surface area between 500 °C to 900 °C). Moreover, temperature programmed reduction (TPR) analysis has shown that for Co/ZrO catalysts a reduction peak has shifted toward the low temperature region when increasing the calcination temperature indicating a more reducible metal phase when calcining at low temperatures. According to the temperature programmed oxidation (TPO) and TEM images that were performed on the spent catalyst, the type of the carbonaceous residue formed for each support (i.e., ZrO<sub>2</sub> and CeO<sub>2</sub>) was different. The presence of CNTs with different sizes was observed for the case of Co/ZrO<sub>2</sub> whereas a reactive carbon was deposited on CeO<sub>2</sub> after the DRM reaction, which has then oxidized due to the high oxygen storage capacity of CeO<sub>2</sub>. To further understand the catalytic activity of Co/CeO<sub>2</sub> catalyst, a similar study was conducted by Ayodele et al. [40] to investigate the impact of the reactants partial pressure on the catalytic performance. It was found that reactants partial pressure of 45 kPa was optimum with about 80% CH<sub>4</sub> conversion and H<sub>2</sub>/CO ratio close to unity. Detailed characterizations of the as-prepared catalysts revealed the excellent dispersion of Co with nanosized particle size on the CeO<sub>2</sub> surface. A more recent study by the same group [41] has reported that the BET surface area of the 20 wt % Co/80 wt % CeO<sub>2</sub> is almost double of the pristine CeO<sub>2</sub> support which implies the good dispersion of Co metals. Other support materials are also reported in literature as excellent candidates that are considered for Co-based catalysts, such as Nd<sub>2</sub>O<sub>3</sub> [42], La<sub>2</sub>O<sub>3</sub> [43], and MgO [44]. A common observation was realized on most of the Co-based systems, regarding the noticeable improvement in the catalyst textural properties after the impregnation of up to 20 wt % Co into the support surface. This could be mainly ascribed to the good dispersion of Co species in the support matrix and the formation of uniform mesopores thereby enhancing the distribution of Co metals. For instance, the bare La<sub>2</sub>O<sub>3</sub> has a total BET surface area of 8 m<sup>2</sup>/g as determined from the N<sub>2</sub>-adsorption-desorption experiment at 77 K which was doubled upon the introduction of 20 wt % Co/80 wt % La<sub>2</sub>O<sub>3</sub> [43]. Similarly, the pristine Nd<sub>2</sub>O<sub>3</sub> surface area was almost tripled from 6.7 m<sup>2</sup>/g upon the impregnation of 20 wt % Co into the support surface [42]. To address the catalyst deactivation issue of Co-based catalysts Mirzaei et al. [44] has impregnated 5–30 wt % Co into MgO supports using co-precipitation method. TEM images have revealed that a small spherical Co particles (10 nm) were identified and the formation of Co-Mg solid solution with reduction temperature greater than 400 °C was confirmed using H<sub>2</sub>-TPR. The catalyst that was prepared at 10 wt % Co loading was found to show 67% CH<sub>4</sub> conversion and was stable up to 15 h at 700 °C. A deeper look at the SEM image (Figure 3) of 10 wt % Co/MgO clearly shows the formation of whisker type coke that did not hindered the accessibility of the reactant feed to the active Co sites [44]. As discussed previously for the case of

Ni/MgO, the basicity of the MgO support that induces the adsorption of CO<sub>2</sub> combined with its high surface area are the main features for their deployment as a stable supports in DRM [14].



**Figure 3.** SEM image of the spent 10 wt % Co/MgO catalyst after 15 h reaction at 700 °C. Reproduced with permission from [44]. (a) Low magnification; (b) high magnification.

**Table 2.** Co-based catalysts and noble metal catalysts for DRM.

Metal	Support	Temperature (K)	CH <sub>4</sub> Conversion	H <sub>2</sub> /CO	Remarks	Ref.
Co	Ca-AC	1173	94		The co-impregnation of Ca on the surface of AC has enhanced the Co-AC interaction, Co dispersion and induced CO <sub>2</sub> adsorption properties resulting in an improved stability	[45]
Co	Nd <sub>2</sub> O <sub>3</sub>	1023	62.7	0.97	Wet impregnation method was used to prepare the catalyst with 20 wt% Co loading and a reaction mechanism was proposed and modelled	[42]
Co	La <sub>2</sub> O <sub>3</sub>	1023	50		Wet impregnation technique was used to prepare the catalysts up to 20 wt % Co loading. The DRM kinetics was modelled using Langmuir-Hinshelwood mechanisms with excellent agreement	[43]
Co	CeO <sub>2</sub>	1023	79.5	0.97	Wet impregnation was employed as a synthesis method achieving enhanced catalytic activity due to the excellent metal dispersion	[41]
Co	CeO <sub>2</sub>	1023	78		The effect of the reactants partial pressure on the catalytic performance was investigated	[40]
Co	Al <sub>2</sub> O <sub>3</sub>	973	61		Catalysts with low metal loadings were investigated for DRM	[46]
Co	MgO	973	69.38	0.79	Co-precipitation technique was used to prepare nanosized catalysts for DRM and the metal loading was optimized	[44]
Ir	Ce <sub>0.9</sub> Pr <sub>0.1</sub> O <sub>2</sub>	1025	62	0.98	Different synthesis strategies were analyzed to control the Ir dispersion, and it was found that deposition-precipitation possesses the lowest coke deposition	[47]
Ru	γ-Al <sub>2</sub> O <sub>3</sub> MgAl <sub>2</sub> O <sub>4</sub> Mg <sub>3</sub> AlO MgO	1023	67 75 80 86		The influence of the support on the metal dispersion was analyzed and it was found that the MgAlO mixed oxide support has excellent stability due to the strong basicity of the support	[48]
Rh	La <sub>2</sub> O <sub>3</sub> -γ-Al <sub>2</sub> O <sub>3</sub>				The effect of phosphorous addition to the support was studied under different impregnation scenarios to study the impacts on catalyst activity and stability	[49]

Table 2. Cont.

Metal	Support	Temperature (K)	CH <sub>4</sub> Conversion	H <sub>2</sub> /CO	Remarks	Ref.
Rh	$\gamma$ -Al <sub>2</sub> O <sub>3</sub>	1073	97.5		Numerical simulation of the catalytic DRM in a membrane reactor was performed to find the optimum operating conditions and it was found that Ni/La <sub>2</sub> O <sub>3</sub> is the most stable catalyst at 1073 K	[50]
Pt	hydroxyapatite (HAP)	973	30	0.92	Different synthesis methods were deployed to introduce Pt into HAP and it was concluded that the incipient wetness is the most efficient technique	[51]

Noble metal catalysts, including Rh, Ru, Pt, Pt, and Ir have also gained considerable attention in the past few years as effective catalysts for DRM, as reported in Table 2. A series of Ru-based catalysts were prepared on different support materials and the metal dispersion was found to be in the following order Ru/Mg<sub>3</sub>(Al)O > Ru/MgO > Ru/MgAl<sub>2</sub>O<sub>4</sub> > Ru/ $\gamma$ -Al<sub>2</sub>O<sub>3</sub>, thereby Ru/Mg<sub>3</sub>(Al)O and Ru/MgO has shown superior catalytic activity and stability than the other supports. Amongst the studied catalysts Ru/Mg<sub>3</sub>(Al)O has shown the highest surface area and metal dispersion of 128 m<sup>2</sup>/g and 15%, respectively. The high dispersion of Ru particles on the Mg<sub>3</sub>(Al)O support resulted in higher metal-support interaction as was manifested in the XPS results that recorded a binding energy of 279.6 eV for Ru/ $\gamma$ -Al<sub>2</sub>O<sub>3</sub> as compared to 280.7 eV for Ru/Mg<sub>3</sub>(Al)O. Figure 4 shows the catalytic performance of these catalysts at various temperatures. In order to further understand the superior performance of Ru/Mg<sub>3</sub>(Al)O catalyst, CO<sub>2</sub>-TPD experiments were performed in the temperature range from 100 °C to 800 °C. Moreover, Ru/Mg<sub>3</sub>(Al)O catalyst was proven to be stable up to 300 h at 750 °C maintaining 80% and 0.9 CH<sub>4</sub> conversion and H<sub>2</sub>/CO ratio, respectively. The presence of Mg<sup>2+</sup> -O<sup>2-</sup> on Ru/Mg<sub>3</sub>(Al)O as compared to Ru/ $\gamma$ -Al<sub>2</sub>O<sub>3</sub> has resulted in a shift in the CO<sub>2</sub> desorption peaks toward higher temperatures, indicating a stronger basicity of the Ru/Mg<sub>3</sub>(Al)O catalyst that plays an important role in the activation of CO<sub>2</sub> during the DRM reaction. The basic nature of the Mg<sub>3</sub>(Al)O and MgO supports was considered to be responsible for the observed catalytic activity and stability, which acts as active sites to adsorb CO<sub>2</sub> and suppress the coke formation through hydrogenation pathway [39].

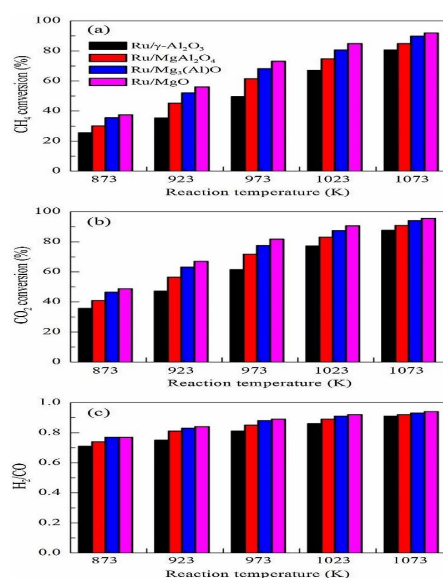


**Figure 4.** Catalytic performance of Ru-based catalysts impregnated on different supports for DRM at different reaction temperatures: (a) CH<sub>4</sub> conversion; (b) CO<sub>2</sub> conversion; and (c) H<sub>2</sub>/CO ratio. Reaction conditions: CH<sub>4</sub>:CO<sub>2</sub>:N<sub>2</sub> = 1:1:2, WHSV = 60,000 mL g<sup>-1</sup> h<sup>-1</sup>; reaction time, 1 h at each temperature; catalyst, 50 mg, pre-reduced with H<sub>2</sub> at 873 K for 0.5 h. Reproduced with permission from [48].

### 2.1.2. Bimetallic Catalysts

The combination of two metals to form bimetallic systems is reported in literature as an efficient approach to improve the catalytic performance in hydrogen production from reforming reactions [52], and it has been concluded that bimetallic catalysts significantly enhance the catalyst lifetime when compared to monometallic catalysts [53]. The physicochemical properties of 5 wt % Ni-10 wt % Co/ $\text{Al}_2\text{O}_3$  catalyst prepared via co-impregnation method were examined and its catalytic performance in DRM was evaluated by Siang et al. [54]. The formation of NiO,  $\text{Co}_3\text{O}_4$ ,  $\text{NiCo}_2\text{O}_4$ ,  $\text{CoAl}_2\text{O}_4$ , and  $\text{NiAl}_2\text{O}_4$  phases was confirmed using XRD analysis leading to  $\text{CH}_4$  conversion and  $\text{H}_2/\text{CO}$  ratio of 67% and 1, respectively, at 700 °C. This was mainly attributed to the fine dispersion of nanosized Ni and Co oxides into the  $\text{Al}_2\text{O}_3$  surface dictating the strong metal-support interaction. To further explain the observed catalytic activity, Raman spectroscopy and SEM scans were utilized to determine the nature of the coke deposited on the spent catalyst. The presence of a whisker type carbon was identified, which in contrary to crystalline carbon, is reactive and did not hinder the accessibility of gaseous reactants to the active metal sites [54]. A similar study by Uner and coworkers has demonstrated the formation of different types of carbonaceous residues on the spent catalyst surface of 8 wt % Ni-4 wt % Co/ $\text{CeO}_2$  [16]. Despite the addition of Co into the Ni/ $\text{CeO}_2$  catalyst, it did not show any improvement in the  $\text{CH}_4$  conversion, however the prolonged catalyst lifetime was realized. This could be explained by the reduction in surface area upon the introduction of Co into the Ni/ $\text{CeO}_2$  matrix. The morphology of the carbonaceous residue was analyzed on the spent catalyst using TEM analysis. A strong metal-support interaction was deduced from the TEM analysis which was deemed responsible for decreasing the catalytic activity in DRM due to the migration of parts of the Ce support to the metal surface during the catalyst reduction stage causing the blockage of the active metals during the reaction. This implies that  $\text{CeO}_2$  works well as a promotor for Ni/ $\text{Al}_2\text{O}_3$ , rather than a support material. A more systematic study is still required to investigate the effect of Co loading in Ni-Co/ $\text{CeO}_2$  catalyst in order to establish the optimum loadings for  $\text{CH}_4$  conversion. Furthermore, increasing the calcination temperature of the bimetallic catalyst has shown a positive impact on lowering coke deposition. High calcination temperature (i.e., 900 °C) has produced one type of amorphous carbonaceous residue which oxidized at 525 °C whereas low calcination temperature (i.e., 700 °C) has produced two different types of coke residues, thus supporting previous findings [16]. In addition to the effect of calcination temperature, catalyst reduction time was also reported to have a great influence on the physicochemical properties of the bimetallic Ni-Co catalyst supported on MgO [55]. 8 wt % Ni-2 wt % Co/MgO Catalyst with shorter reduction times (i.e., less than 1 h) exhibited better catalytic activity than catalyst reduced for long times, mainly due to the formation of smaller metal sites with excellent dispersion (10%) after short reduction times while the long exposure to reducing environment has resulted in metal agglomeration, and hence the catalyst was susceptible to deactivation. The proven effects of catalyst calcination temperature and reduction time on the characteristics and performance of the resulting catalyst brings the attention to the role of the synthesis method in general. Haghghi group has investigated the use of sonochemical, sequential impregnation, and sol-gel synthesis methods in the preparation of Ni-Co/ $\text{Al}_2\text{O}_3$ - $\text{ZrO}_2$  catalysts for DRM [37,56]. The use of ultrasound irradiation assisted impregnation is proven effective to overcome the agglomeration of metals and achieve a good metal dispersion, uniformity of metal distribution, and high specific surface area, and therefore high conversion and stability were attained. The effects of ultrasound power and time on the metal dispersion were significant, as indicated by the TEM images of the 10 wt % Ni-3 wt % Co/ $\text{Al}_2\text{O}_3$ - $\text{ZrO}_2$  catalysts that were prepared at different ultrasonic power and durations. A closer look at the  $\text{H}_2$ -TPR indicates that the presence of Co and  $\text{ZrO}_2$  has improved the Ni- $\text{Al}_2\text{O}_3$  interactions by preventing the formation of the inactive  $\text{NiAl}_2\text{O}_4$  spinals. Furthermore, the use of sonication assisted impregnation has resulted in a more sharp peaks in the  $\text{H}_2$ -TPR profiles opposed to wider peaks for the regular impregnation samples, dictating a narrow size distribution of the Ni and Co metals, and consequently a stronger metal-support interaction. The superior coke suppression property of the ultrasound-modified samples (stable up to 24 h) could

be mainly ascribed to the excellent dispersion and small metal sizes induced by the ultrasound power [56]. The excellent coking suppression property of the Ni-Co/ $\text{Al}_2\text{O}_3$ - $\text{ZrO}_2$  samples that were prepared using ultrasonic method (denoted as NiCoAZ-U) as compared to the wet impregnation route (NiCoAZ-I) was confirmed from the TGA profiles, as shown in Figure 5. Interestingly, there was a significant weight loss that was observed for NiCoAZ-I in the temperature zone from 500 °C to 700 °C whereas no weight loss was noticed for NiCoAZ-U given the fact that the weight loss between 500 °C to 700 °C is attributed to the oxidation of coke to  $\text{CO}_2$  and CO. The SEM images (not shown here) have also confirmed the findings from TGA results indicating no coke formation up to 24 h at reaction temperature of 850 °C. Similar observations were reported for the impregnation of Ni-Co on zeolite Y using ultrasound irradiation assisted impregnation. The superior catalytic activity Ni-Co/ $\text{Al}_2\text{O}_3$ - $\text{ZrO}_2$  and Ni-Cu/ $\text{Al}_2\text{O}_3$ - $\text{ZrO}_2$  catalysts prepared using sol-gel synthesis approach in contrast to sequential impregnation method was also attributed to the metal dispersion and particle size differences [37]. It is also worthy to mention that the addition of Co had greater impacts on the catalyst activity when compared to Cu promoters, mainly due to the higher surface area of the Co-Ni bimetallic system than the Cu-Ni catalysts and consequently the reactants adsorption. To further prolong the lifetime of Ni-Co bimetallic catalysts, Pintar et al. [57] has recently proposed the coating of the bimetallic Ni-Co/ $\text{CeO}_2$ - $\text{ZrO}_2$  catalyst onto the surface of  $\beta$ -SiC to achieve a stable performance up to 550 h, as can be seen in Figure 6. The introduction of  $\beta$ -SiC provided a mean to control the extent of oxygen mobility induced by the  $\text{CeO}_2$ - $\text{ZrO}_2$  support and could be used to tune the redox property of the catalyst and consequently attain higher stability.

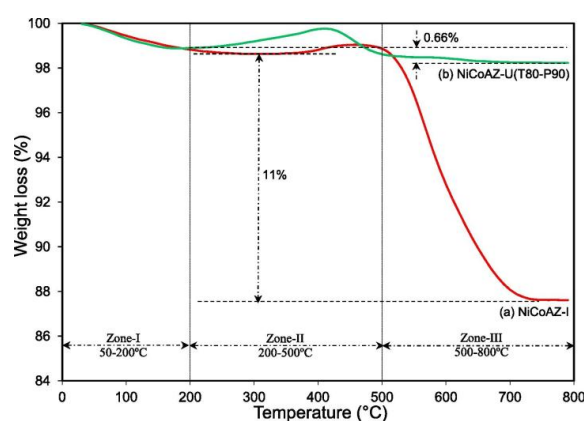


**Figure 5.** Thermogravimetric Analysis (TGA) profile of the spent NiCoAZ catalyst prepared using (a) Wet impregnation route and (b) Ultrasound irradiation method. Reproduced with permission from [56].

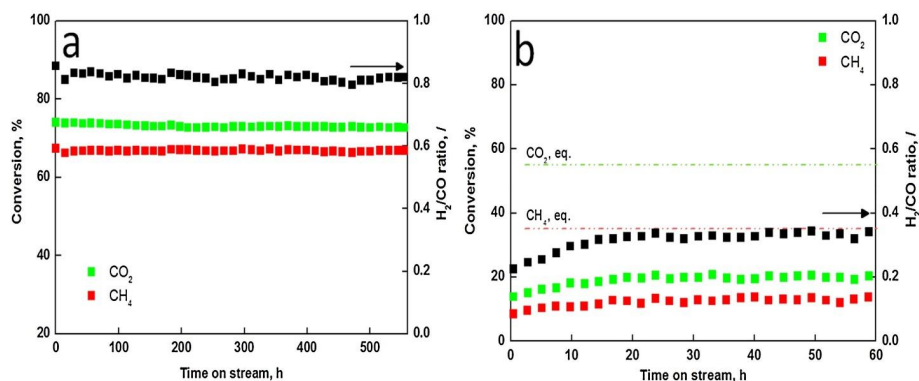


**Figure 6.**  $\text{CH}_4$ ,  $\text{CO}_2$  conversion and  $\text{H}_2/\text{CO}$  ratio of 3 wt % NiCo/ $\text{CeO}_2$ - $\text{ZrO}_2$  at 750 °C and (a) 1.2 bar and (b) 20 bar. Reproduced with permission from [57].

Other bimetallic catalytic systems that are reported in literature are summarized in Table 3.

Mesoporous silica SBA-15 with hexagonal one-dimensional pore structures was also proven to be a promising support for Ni-Co bimetallic systems [58,59]. Figure 7 displays the effect of Co/Ni ratio in the  $Ni_xCo_{1-x}/SBA-15$  catalyst at two GHSV of 36,000 mL/g/h and 72,000 mL/g/h [58]. It was found that at lower GHSV (i.e., 36,000 mL/g/h) the addition of Co has shown a negative effect on the  $CH_4$  and  $CO_2$  conversion as compared to the monometallic Ni/SBA-15 catalyst. However, as the GHSV was increased to 72,000 mL/g/h, the catalytic activity of the bimetallic  $Ni_xCo_{1-x}/SBA-15$  catalyst was even higher than the monometallic Ni/SBA-15 catalyst. Especially for the sample with the lowest CO/Ni ratio ( $Ni_9Co_1/SBA-15$ ). To explain the positive role of Co addition to the  $Ni_xCo_{1-x}/SBA-15$  catalyst, the particle sizes of the samples are plotted against the initial DRM activity, as shown in Figure 7c. It was concluded that the introduction of Co induces the formation of Co-Ni alloys, and hence leading to smaller Ni particle sizes, especially at low Co/Ni ratios confirming previous findings [59].

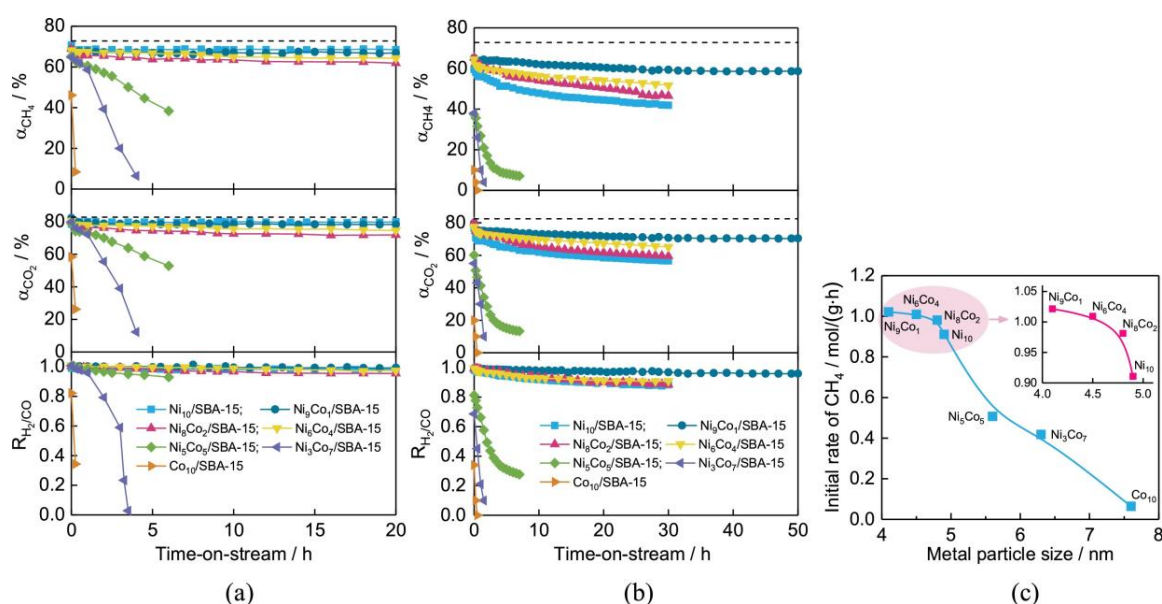


**Figure 7.** Catalytic activity of various  $Ni_xCo_{1-x}/SBA-15$  catalysts at 973 K and (a) GHSV = 36,000 mL/g/h and (b,c) 72,000 mL/g/h. Reproduced with permission from [58].

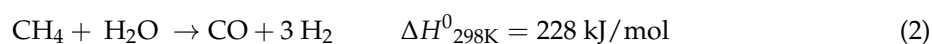
A recent study has studied the controlled deposition of Fe-Ni nanoparticles onto Mg(Al)O periclase support using colloid synthesis route [60]. According to energy dispersive X-ray analysis (EDX) and X-ray absorption near-edge structure (XANES), the formation of a core-shell structure was confirmed with the Ni in the core and Fe in the shell side. The DRM reaction was performed at 650 °C, and it was found that the rate of  $CH_4$  consumption was 10 times higher in the pure Ni catalyst when compared to the Ni/MgAlO prepared using coprecipitation route. However, the pure Ni nanoparticles have suffered a severe deactivation via carbonaceous residue formation. For the case of the bimetallic Ni-Fe catalyst, and optimum ratio of Ni/Fe of 3:1 was found to produce a catalyst with high active metal sites and improved stability. It was also found that the selection of the catalyst reduction temperature is critical to prolong the catalyst lifetime. For instance, catalysts reduced at 650 °C as opposed to 850 °C has shown a decrease in coke formation by up to 50%, as was measured by the TPO experiments. In order to further understand the synergism in Ni-Fe bimetallic systems and in order to understand the mechanism through which the Ni-Fe alloys function, the reader is advised to refer to the work by Kim et al. [61].

Table 3. Bimetallic catalyst systems for DRM.

Metal	Support	Temperature (K)	CH <sub>4</sub> Conversion	H <sub>2</sub> /CO	Remarks	Ref.
Ni-Co	CeZrO <sub>2</sub> /β-SiC	1023	65	0.8	Deposition precipitation was used to produce catalyst with controlled metal cluster size to reduce coking	[57]
Ni-Co	γ-Al <sub>2</sub> O <sub>3</sub>	973	67	1	The bimetallic catalyst with small crystallite size was prepared using to improve the catalyst activity and stability. The formation of an amorphous carbon was evident explaining the catalyst prolonged lifetime	[54]
Ni-Co	ZrO <sub>2</sub> -Al <sub>2</sub> O <sub>3</sub>	1123	93	1	The ultrasound-mediated synthesis produced catalysts with high surface area, small crystal size, and high metal dispersion resulted in the observed enhanced stability	[56]
Ni-Co	CeO <sub>2</sub>	973	64	0.80	The effects of the catalyst calcination temperature on the catalytic activity and stability was studied, and it was certain that at higher calcination temperatures the carbon deposition was minimized	[16]
Co-Ce	ZrO <sub>2</sub>	973	78	0.67	The oxygen storage property of the ZrO <sub>2</sub> support was promoted by adding Ce at different ratios to reduce metal sintering and carbon formation	[62]
Ni-Co	ZSM-5	1073	80	0.98	Introducing Co to Ni/ZSM-5 catalyst has significantly improved the catalyst stability due to the activity of Co in oxidation reactions	[47]
Ni-Co	Zeolite Y	1123	96	0.93	The utilization of ultrasonic power in the synthesis of Co-Ni bimetallic catalyst has resulted in higher metal dispersion	[63]
Co-Mo	MgO/MWCNTs	1223	98.6	1.1	The insitu growth of multiwall carbon nanotubes (MWCNTs) in the solution of mixed Co and Mo precursors was used to prepare the composite catalyst with excellent activity for syngas production	[64]
Ni-Co	CeO <sub>2</sub> -ZrO <sub>2</sub>	973	90	0.73	The mixed support was prepared by thermal precipitation in ethylene glycol media	[65]
Ni-Cu	Al <sub>2</sub> O <sub>3</sub>	1123	82	0.83	Plasma treatment was applied to synthesize the bimetallic nanocatalysts to improve the uniformity of metal dispersion	[66]
Ni-Co	MgO	1073	92	0.98	The impacts of the catalyst reduction duration was studied and it was concluded that the short reduction time is preferable for better stability	[55]
Mn-Ni	SiO <sub>2</sub>	1073	77.8	0.65	The positive impact of Mn as a catalyst promotor was confirmed	[67]
Zr-Ni	SiO <sub>2</sub>	1073	89.3			
Co-Sr	γ-Al <sub>2</sub> O <sub>3</sub>	973	80	0.88	The Sr acted as a promotor to enhance the support basicity and hence reduced carbon formation with no effects on the catalytic activity	[68]
Pt-Ni	Al <sub>2</sub> O <sub>3</sub>	1073	92	1.1	The role of the addition of Pt to the Ni-based catalyst was analyzed using two oxide supports. The improvement in the catalyst lifetime was highly pronounced when adding Pt to Ni/CeZrO <sub>2</sub>	[38]
Pt-Ni	CeZrO <sub>2</sub>	1073	94	0.8		
Ni-Co	Al <sub>2</sub> O <sub>3</sub> -ZrO <sub>2</sub>	1123	96	0.98	The effects of synthesis method and the use of metal promoters was investigated	[37]
Ni-Cu	Al <sub>2</sub> O <sub>3</sub> -ZrO <sub>2</sub>	1123	93	0.93		

## 2.2. Steam Reforming of Methane (SRM)

Syngas production from SRM is one of the very well established technologies that is available in commercial scales using mainly Ni/Al<sub>2</sub>O<sub>3</sub> catalysts in reformers operated at high temperatures (i.e., 800 °C) [69]. In this review article we have limited our literature to include only scientific publications available after 2013 to recapitulate the advancement achieved in the catalyst development for SRM. The SRM is a highly endothermic reaction and to attain a high CH<sub>4</sub> conversion and H<sub>2</sub>/CO ratio the reaction should be operated at elevated temperatures and high H<sub>2</sub>O/CH<sub>4</sub> ratios which present great challenges such as the high energy requirements and the necessity for desulfurization prior to entering the reformer.



According to the SRM reaction, the produced syngas has H<sub>2</sub>/CO ratio of 3:1, which makes it suitable for hydrogen production for fuel cell applications. Table 4 presents a summary of the recent advances in the catalyst development for SRM in the past five years.

Table 4. Summary of Catalysts used for steam reforming of methane (SRM).

Catalyst	CH <sub>4</sub> Conversion %	Conditions	Catalyst Characteristics	Remarks	Ref.
10 wt % Ni/SiO <sub>2</sub>	35	700 °C, 3.5 h, H <sub>2</sub> O/CH <sub>4</sub> = 0.5	Ni particle size = 6.9 nm	The catalyst prepared using plasma was evaluated for long-term stability	[70]
10 wt % Ni/TiO <sub>2</sub>	27	500 °C, H <sub>2</sub> O/CH <sub>4</sub> = 1	BET surface area = 42 m <sup>2</sup> /g and Ni dispersion = 2.8%	Different Ni contents were loaded on TiO <sub>2</sub> for SRM at low temperatures	[71]
10 wt % Ni/Al <sub>2</sub> O <sub>3</sub>	30	500 °C, H <sub>2</sub> O/CH <sub>4</sub> = 1	BET surface area = 40 m <sup>2</sup> /g and Ni dispersion = 1.3%		
10 wt % Ni/SiO <sub>2</sub>	10	500 °C, H <sub>2</sub> O/CH <sub>4</sub> = 1	BET surface area = 300 m <sup>2</sup> /g and Ni dispersion = 2.6%		
10 wt % Ni/SiO <sub>2</sub>	96	700 °C, H <sub>2</sub> O/CH <sub>4</sub> = 3.5	BET surface area = 268 m <sup>2</sup> /g and particle size = 11 nm	The sol-gel technique was used to prepare the catalyst with small particle sizes	[72]
15 wt % Ni/TiO <sub>2</sub>	92	700 °C, H <sub>2</sub> O/CH <sub>4</sub> = 1.2	BET surface area = 62 m <sup>2</sup> /g	Ultrasound irradiation was used to enhance the Ni dispersion	[73]
15 wt % Ni/MgAl <sub>2</sub> O <sub>4</sub>	45	600 °C, 5 bar, H <sub>2</sub> O/CH <sub>4</sub> = 5	BET surface area = 43 m <sup>2</sup> /g, Ni dispersion = 6.3%, and particle size = 10 nm	The effect of calcination temperature on the physicochemical properties was analyzed	[74]
9 wt % Ni/ZrO <sub>2</sub>	65	973 K and, H <sub>2</sub> O/CH <sub>4</sub> = 4	BET surface area = 19 m <sup>2</sup> /g and particle size = 23 nm	Different structures of ZrO <sub>2</sub> supports were used for SRM	[75]
6 wt % Ni/ZrO <sub>2</sub>	30	650 °C and, H <sub>2</sub> O/CH <sub>4</sub> = 2.5	BET surface area = 16 m <sup>2</sup> /g	The textural properties of ZrO <sub>2</sub> support were controlled to improve Ni dispersion	[76]
Ni/SiO <sub>2</sub> /ZrO <sub>2</sub>	95	650 °C and, H <sub>2</sub> O/CH <sub>4</sub> = 2.5	BET surface area = 176 m <sup>2</sup> /g		
10 wt % Ni/Y <sub>2</sub> Zr <sub>2</sub> O <sub>7</sub>	85	700 °C and, H <sub>2</sub> O/CH <sub>4</sub> = 2	BET surface area = 21 m <sup>2</sup> /g and particle size = 12 nm and Ni dispersion = 100%	Different synthesis approaches were used to prepare the support which showed different metal-support interactions	[77]
Ni/Al <sub>2</sub> O <sub>3</sub> -Silicalite	69	650 °C, and H <sub>2</sub> O/CH <sub>4</sub> = 3		The silicalite shell was grown around Al <sub>2</sub> O <sub>3</sub> followed by impregnation to introduce Ni into the core of the catalyst	[78]
Ni/90 wt % Ce-10 wt % Gd	73	700 °C, and H <sub>2</sub> O/CH <sub>4</sub> = 3	BET surface area = 65 m <sup>2</sup> /g and metal dispersion = 1.6%	Doping the support with Gd improved H <sub>2</sub> /CO ratio at the expense of the catalytic activity	[79]
Ni/MgAl	40	600 °C, and H <sub>2</sub> O/CH <sub>4</sub> = 2	BET surface area = 97 m <sup>2</sup> /g and particle size = 14 nm	Ni-based hydrotalcite catalyst was prepared and the use of Fe and Cr promoters on the Ni dispersion was studied.	[80]
Fe-Ni/MgAl	50	600 °C, and H <sub>2</sub> O/CH <sub>4</sub> = 2	BET surface area = 98 m <sup>2</sup> /g and particle size = 8 nm		
Cr-Ni/MgAl	45	600 °C, and H <sub>2</sub> O/CH <sub>4</sub> = 2	BET surface area = 104 m <sup>2</sup> /g and particle size = 8 nm		
Ni/MgAl + CrFe <sub>3</sub> O <sub>4</sub>	75	600 °C, and H <sub>2</sub> O/CH <sub>4</sub> =2	BET surface area = 13 m <sup>2</sup> /g		
13 wt % Ni-1 wt % Ce/Al <sub>2</sub> O <sub>3</sub>	75	750 °C, and H <sub>2</sub> O/CH <sub>4</sub> = 3	BET surface area = 26 m <sup>2</sup> /g and Ni dispersion = 8.3%	The effects of Ce as a promoter for Ni-based catalyst was investigated	[81]
5 wt % Ni/SiO <sub>2</sub> -Al <sub>2</sub> O <sub>3</sub>	75	750 °C, and H <sub>2</sub> O/CH <sub>4</sub> = 1	BET surface area = 73 m <sup>2</sup> /g and particle size = 19 nm	Ni nanoparticles supported catalysts exhibited better dispersion, particle size, and reducibility than conventional Ni catalysts	[82]
5 wt % Ni nano-particles/SiO <sub>2</sub> -Al <sub>2</sub> O <sub>3</sub>	98	750 °C, and H <sub>2</sub> O/CH <sub>4</sub> = 1	BET surface area = 106 m <sup>2</sup> /g and particle size = 6 nm		
5 wt % Ni/Al <sub>2</sub> O <sub>3</sub> -Y <sub>2</sub> O <sub>3</sub> -ZrO <sub>2</sub>	95	1125 K, and H <sub>2</sub> O/CH <sub>4</sub> = 1.5		SRM was studied at low H <sub>2</sub> O/CH <sub>4</sub> to enhance the energy efficiency	[83]
0.09 wt % (Pd-Rh)/CeZrO <sub>2</sub> -Al <sub>2</sub> O <sub>3</sub>	93	1073 K, and H <sub>2</sub> O/CH <sub>4</sub> = 1.5	BET surface area = 146.8 m <sup>2</sup> /g and metal dispersion = 37.5%	The bimetallic catalyst was coated on metallic foam to reduce coke formation	[84]
8 wt % Rh/Al <sub>2</sub> O <sub>3</sub>	88	1073 K, and H <sub>2</sub> O/CH <sub>4</sub> = 1.5	BET surface area = 6.4 m <sup>2</sup> /g		
13 wt % Ni/Al <sub>2</sub> O <sub>3</sub>	85	1073 K, and H <sub>2</sub> O/CH <sub>4</sub> = 1.5	BET surface area = 164 m <sup>2</sup> /g		
0.1 wt % Pt-13 wt % Ni/MgAl <sub>2</sub> O <sub>4</sub>	65	600 °C, and H <sub>2</sub> O/CH <sub>4</sub> = 5	BET surface area = 44 m <sup>2</sup> /g and particle size = 7.6 nm	The catalyst reducibility was improved by doping the catalyst with different Pt loadings	[85]
5 wt % Ir/MgAl <sub>2</sub> O <sub>4</sub>	55	850 °C, and H <sub>2</sub> O/CH <sub>4</sub> = 3	particle size = 1 nm and metal dispersion = 100%	Ir and Rh supported on MgAl <sub>2</sub> O <sub>4</sub> were found to have high metal dispersion and hence better catalytic activity	[86]
5 wt % Rh/MgAl <sub>2</sub> O <sub>4</sub>	41	850 °C, and H <sub>2</sub> O/CH <sub>4</sub> = 3	particle size = 2 nm and metal dispersion = 50%		
5 wt % Pt/MgAl <sub>2</sub> O <sub>4</sub>	49	850 °C, and H <sub>2</sub> O/CH <sub>4</sub> = 3	particle size = 3 nm and metal dispersion = 29%		
5 wt % Pd/MgAl <sub>2</sub> O <sub>4</sub>	31	850 °C, and H <sub>2</sub> O/CH <sub>4</sub> = 3	particle size = 16 nm and metal dispersion = 6%		
5 wt % Ru/MgAl <sub>2</sub> O <sub>4</sub>	3	850 °C, and H <sub>2</sub> O/CH <sub>4</sub> = 3	particle size = 20 nm and metal dispersion = 5%		
5 wt % Ni/MgAl <sub>2</sub> O <sub>4</sub>	4	850 °C, and H <sub>2</sub> O/CH <sub>4</sub> = 3	particle size = 7 nm and metal dispersion = 15%		
1 wt % Pt/Al <sub>2</sub> O <sub>3</sub>	70	973 K, and H <sub>2</sub> O/CH <sub>4</sub> = 4	BET surface area = 131 m <sup>2</sup> /g and metal dispersion = 50%		
1.4 wt % Pt/CeO <sub>2</sub> -Al <sub>2</sub> O <sub>3</sub>	75	973 K, and H <sub>2</sub> O/CH <sub>4</sub> = 4	BET surface area = 84 m <sup>2</sup> /g and metal dispersion = 83%	The effect of the addition of toluene to the feed stream was studied	[87]

The catalytic performance of different Ni-based catalysts that were prepared using incipient wetness impregnation ( $\text{SiO}_2$ ,  $\text{Al}_2\text{O}_3$ ) and co-precipitation technique (Mg-Al and Zn-Al) was evaluated for SRM at low temperature (less than  $600\text{ }^\circ\text{C}$ ) by Nieva et al. [88]. The catalysts prepared via the co-precipitation route (Ni/Mg-Al and Ni/Zn-Al) was found to have better activity and stability compared to Ni/ $\text{SiO}_2$  and Ni/ $\text{Al}_2\text{O}_3$  samples due to the higher metal-support interactions of these catalysts. The superior catalytic activity could be attributed to the small particle sizes recorded for Ni/Mg-Al (3 nm) and Ni/Zn-Al (6 nm) as compared to the larger particle sizes measured using TEM histograms for Ni/ $\text{SiO}_2$  (12 nm) and Ni/ $\text{Al}_2\text{O}_3$  (19 nm) samples. The small particle size and the strong metal-support interaction for Ni/Mg-Al and Ni/Zn-Al have prevented the dissolution of carbon, and thus the formation of nanofibers as was evident from TGA analysis. Moreover, the inhibition of  $\text{CH}_4$  decomposition and CO disproportionation reactions combined with the fast gasification of coke on Ni/Mg-Al and Ni/Zn-Al is deemed responsible for the observed stability. Another comparison between the different support materials for SRM was conducted recently and modelled using artificial neural network (ANN) to optimize the Ni loadings and the process operating conditions [89]. The authors have used wet impregnation synthesis method to introduce Ni (5, 10, 20, and 40 wt %) into  $\text{SiO}_2$ ,  $\text{Al}_2\text{O}_3$  and SBA-15 supports promoted with 1 wt % Ce, Mo, B and Zr. The catalyst prepared with 10 wt % Ni on SBA-15 support has shown the highest activity and coke resistance compared to the other catalysts. The promotion of 10 wt % Ni/SBA-15 with 1 wt % Ce was found to further improve the catalyst stability and increase the  $\text{CH}_4$  reaction rate. This is mainly attributed to the small particle sizes (11 nm), good Ni dispersion (10%), and the excellent oxygen storage capacity of Ce promoters [81]. The excellent textural properties of SBA-15 (BET surface area of  $300\text{ m}^2/\text{g}$  and pore volume of  $0.6\text{ cm}^3/\text{g}$ ) provided a large surface for Ni deposition without any agglomeration, similar to previous findings [13,76]. Mesoporous silica (MCM-41) possesses hexagonal pores with similar textural properties as SBA-15 have been also studied as a promising candidate for Ni supported catalysts in SRM. As an attempt to reduce the Ni particle size the use of sol-gel synthesis method for the preparation of Ni/ $\text{SiO}_2$  catalysts was investigated in comparison to conventional impregnation methods [90]. It was found that the sol-gel (also called polymer-assisted synthesis) produces small and well-dispersed Ni particles, and hence has high metal-support interactions thereby having longer lifetime in SRM up to 60 h. The measurement of crystallite size using XRD diffractograms revealed the importance impact of the synthesis route on the size of NiO crystallites. Much smaller crystallites (8–11 nm) are deposited using polymer-assisted approach when compared to conventional impregnation (15–23 nm), which could be ascribed to the formation of very small NiO particles prior to the combustion of the polymer matrix, which has then firmly attached afterwards on the  $\text{SiO}_2$  support. Furthermore, the small particle size on the calcined catalyst obtained using the sol-gel method were retained after the reduction step at  $750\text{ }^\circ\text{C}$ , while for the case of impregnation routes, the particle sizes have further increased up to 45 nm. To differentiate between the amount and types of carbonaceous residues formed on the spent catalysts that were prepared via conventional impregnation and sol-gel technique, TPO analysis was performed. It was concluded that mainly amorphous carbon (less deactivating) was deposited on the sol-gel catalyst while a graphitic coke (more crystalline phase) was formed on the catalyst prepared via the impregnation route [90]. Another attempt to prepare Ni nanoparticle using sol-gel synthesis approach was reported by Ali and coworkers [82] for the impregnation of 5 wt % Ni into the surface of 10 wt %  $\text{SiO}_2$  modified alumina support. The as-synthesized Ni nanoparticles exhibited exceptionally superior catalytic activity and stability compared to the conventionally impregnated catalysts mainly due to the better dispersion, high reducibility, and the smaller particle sizes (6 nm as opposed to 19 nm for the conventional impregnation samples). Similarly, other researchers have reported the improved characteristics of catalysts prepared via sol-gel route, for instance Bej et al. [72] have varied the catalyst calcination temperature and Ni loading to optimize the NiO crystallite size on a Ni/ $\text{SiO}_2$  catalyst prepared using sol-gel method. Low calcination temperatures (i.e.,  $400\text{ }^\circ\text{C}$ ) was found to produce small Ni particle size recording a  $\text{CH}_4$  conversion of about 96% at  $700\text{ }^\circ\text{C}$  and  $\text{H}_2\text{O}/\text{CH}_4$  ratio of 3.5 stable up to 3 h, confirming previous findings [74]. However, it is worthy to mention that

an optimization of the calcination temperature is always required, due to their impact on the metal particle size and catalyst surface area, and consequently the catalytic performance. Moreover, the use of dielectric barrier discharge plasma (DBC) was found to have similar results to sol-gel synthesis method producing Ni particle sizes of about 5 nm and hence showing better stability in SRM [70]. Furthermore, the use of ultrasound irradiation assisted impregnation method was proven successful to obtain fine metal dispersion of small Ni particles, as was observed for the case of Ni/TiO<sub>2</sub> catalysts [73]. In order to further improve the catalytic performance of Ni/TiO<sub>2</sub> catalysts in SRM, Kho et al. [71] have recently proposed that the activation step for Ni/TiO<sub>2</sub> catalysts should be performed at milder conditions (i.e., less than 400 °C) to avoid undesirable phase changes in TiO<sub>2</sub> support. Findings from this study revealed that for 10 wt % Ni/TiO<sub>2</sub> the presence of two forms of Ni was evident, a bulk-like Ni and a strongly attached Ni-TiO<sub>2</sub>. Each phase has contributed differently in the overall SRM reaction leading to a stable performance up to 54 h at 500 °C. The effect of H<sub>2</sub>O/CH<sub>4</sub> ratio on the catalytic activity and stability of 10 wt % Ni/TiO<sub>2</sub> up to 54 h was assessed in the range from 1 to 3. At values of H<sub>2</sub>O/CH<sub>4</sub> = 1 and 3, the catalyst stability was retained and the values of H<sub>2</sub>/CH<sub>4</sub> and H<sub>2</sub>/Co<sub>x</sub> of approximately 4 was observed. Whereas, at H<sub>2</sub>O/CH<sub>4</sub> = 2, the catalyst lost its stability after 24 h with a slight increase in the H<sub>2</sub>/CH<sub>4</sub> and H<sub>2</sub>/Co<sub>x</sub> ratios to about 5. This observation could be explained from the XRD spectra of the spent catalyst at different H<sub>2</sub>O/CH<sub>4</sub> ratios. An accelerated growth in the Ni particle size was observed up to 7 nm, 12 nm, and 19 nm for H<sub>2</sub>O/CH<sub>4</sub> ratios of 1, 2, and 3, respectively. Moreover, an unfavorable phase transformation from the higher surface area anatase-TiO<sub>2</sub> to rutile-TiO<sub>2</sub> was depicted from the XRD patterns, which could lead to partial activity losses. This can be clearly seen from the weight loss at 700 °C for the spent catalysts at H<sub>2</sub>O/CH<sub>4</sub> ratios higher than 1. These observations indicate the importance of optimizing the operating conditions in SRM reactions.

While Ni-based catalysts received the most attention for industrial SRM applications, the catalyst deactivation through metal sintering and coke deposition is considered the major challenge to be addressed. Noble metals (Pt, Rh, Ru, and Ir) supported on various oxide supports that have been extensively studied in the past for SRM can overcome these shortcomings of Ni-based systems. A series of noble metal catalysts supported on MgAl<sub>2</sub>O<sub>4</sub> and Al<sub>2</sub>O<sub>3</sub> using incipient wetness impregnation method were evaluated for SRM [86]. Exceptionally high metal dispersions were recorded for the case of Ir and Rh (100% and 50%, respectively) with particle sizes less than 2 nm, which was reflected in their superior activity and stability (five times higher than Ni/MgAl<sub>2</sub>O<sub>4</sub>). According to SEM images, the use of MgAl<sub>2</sub>O<sub>4</sub> support produced significantly smaller particle sizes as compared to using Al<sub>2</sub>O<sub>3</sub> which explains the observed reduction in CH<sub>4</sub> conversion from 90% to 78% for 5 wt % Rh/Al<sub>2</sub>O<sub>3</sub> within 70 h, while 5 wt % Rh/MgAl<sub>2</sub>O<sub>4</sub> maintained the same initial conversion of 95%. Implications of density functional theory (DFT) analysis attributed the observed coke resistance property to the presence of a strong positive charge for the case of Rh and Ir supported on MgAl<sub>2</sub>O<sub>4</sub>, which increased the metal-support interaction. To further improve the catalytic performance of Rh-based catalysts, the utilization of a mixed support approach provides a great synergism toward enhancing the overall characteristics of the catalyst in SRM. Duarte et al. [91] has systematically investigated the promotion of Al<sub>2</sub>O<sub>3</sub> support with CeO<sub>2</sub> and Sm<sub>2</sub>O<sub>3</sub>-CeO<sub>2</sub> for SRM at 500 °C. The coexistence of atomically deposited Rh and Rh nanoparticles on the Rh/CeO<sub>2</sub>-Al<sub>2</sub>O<sub>3</sub> has led to a positive synergism toward carbon gasification during SRM, thereby showing only 17% deactivation at 500 °C. Similarly, Castro et al. [87] has investigated the impact of adding CeO<sub>2</sub> to Pt/Al<sub>2</sub>O<sub>3</sub> catalyst to introduce new oxygen vacancies and prolong the catalyst lifetime. The CeO<sub>2</sub> acted as a source of oxygen during the SRM reaction to control the redox property of the catalyst and to induce a balance between the gasification and reforming reactions in a way to suppress coke deposition on the catalyst surface.

Nevertheless, noble metals are expensive and therefore a bimetallic system where noble metals are added to Ni-based systems could provide the ultimate properties due to the formation of superficial Ni-noble metal alloys [92,93]. In order to understand the synergistic effects in Ni-Co bimetallic catalysts in SRM, a series of Ni-Co/Al<sub>2</sub>O<sub>3</sub> catalysts were prepared using co-impregnation technique with Ni content of 12 wt % and different Co loadings (1%, 3%, 7%, 12%, and 15%) [53]. Although, the catalytic

activity of the Co-modified catalysts was decreased compared to the 12 wt % Ni/Al<sub>2</sub>O<sub>3</sub>, the catalyst stability was significantly improved up to 160 h for the case of 7 wt % Co at 800 °C as was confirmed by SEM images of the fresh and spent catalyst. A theoretical study was presented by Wang et al. [94] using DFT to determine the major reactions taking place in bimetallic systems of Ni-catalyst modified with Cu, Au, and Ag in an attempt to determine the least carbon producing bimetallic catalyst and understand the observed experimental findings. More recently, the introduction of 0.01–1 wt % Pt into Ni/MgAl<sub>2</sub>O<sub>4</sub> catalyst prepared using sequential impregnation technique was studied by Jaiswar et al. [85]. Figure 8 shows the CH<sub>4</sub> conversion at different Pt loadings, which correlate very well with the recorded metal specific surface areas of these samples. The optimum Pt loading was found to be 0.1 wt % based on the metal dispersion and catalytic activity, which was ascribed to the increase in metal specific surface area and the formation of Pt-Ni alloys on the catalyst surface. The addition of Pt beyond 0.1 wt % has resulted in agglomeration of the active metals and consequently lowering the catalyst activity and stability, thus, it is always essential to optimize the metal loading in bimetallic systems.

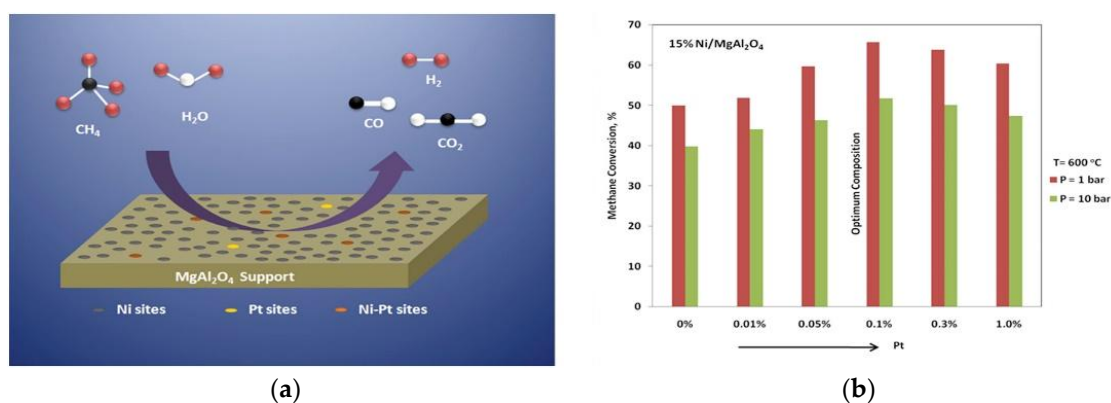


**Figure 8.** Schematic representation of Ni-Pt/MgAl<sub>2</sub>O<sub>4</sub> bimetallic system (a), and the optimum catalytic performance in SRM (b).

### 3. Conclusions

Over the past five years, several studies have been conducted on DRM and SRM over Ni-based metal-oxide catalysts to improve the syngas production rate, while maintaining the catalyst stability. The role of the support was found essential to achieving the required physicochemical properties in syngas production through DRM. Promoting the Al<sub>2</sub>O<sub>3</sub> support with CeO<sub>2</sub>, ZrO<sub>2</sub>, SiO<sub>2</sub>, and La<sub>2</sub>O<sub>3</sub> was found to have significant impacts on the catalyst characteristics, such as the Ni dispersion, particle size, metal specific surface area, and the catalyst reducibility. Therefore, the selection of the right combination of the support material is necessary to maximize syngas production. Although the strong metal-support interaction has led to more stable catalysts for both DRM and SRM applications, the catalyst reducibility has been an issue, therefore a tradeoff between the metal-support interaction and the catalyst reducibility is always required. The support surface acid/base property was also found to be a key factor to control the catalyst stability via the control of the activation energy of the CO<sub>2</sub> and CH<sub>4</sub> reaction pathways. The acid/base property could be controlled using various approaches, such as the calcination temperature, the use of basic supports (such as MgO), the synthesis method, and the acidity modifiers. Furthermore, the control of the metal loading in the catalyst is always required in order to determine the limits where metal agglomeration starts to appear. The most influential factor on the catalyst stability was found to be the metal particle size and dispersion. Preparing nanoparticles through the variation of synthesis methods and conditions is considered to be a promising route to produce catalysts with small particle sizes. It was also concluded that not only the nature of the metal and support are important in DRM and SRM reactions but also the synthesis scheme used to prepare

the catalysts, since all of the properties are greatly dependent on the synthesis conditions and the catalyst formulations. The utilization of different synthesis methods in preparing the catalysts is a potential area of research where great achievement could be realized.

The major challenge for Ni-based catalysts was found to be the deactivation and high coke formation opposed to noble metals, which displayed considerably stable performances. Consequently, future studies in the area of bimetallic systems are very promising to achieve a synergism between transient and noble metals toward high methane conversion and longer stability. Controlling the doping ratio of the noble metal to non-noble metal catalyst is very crucial to achieve the required stability improvement as higher doping percentages can lead to agglomeration and loss of activity. In addition to noble metals, Co has also shown a great potential to improve the stability of the catalyst by creating Ni-Co alloys and reducing the Ni particle sizes especially on large surface area supports such as mesoporous silica (SiO<sub>2</sub>, MCM-41 and SBA-15). However, the optimization of the Ni/Co ratio in the bimetallic catalyst along with the operating conditions is very crucial to obtain the best catalyst formulations and catalytic results.

Furthermore, more detailed characterizations and theoretical calculations that are based on computational analysis are still required to understand the mechanisms behind these observed catalytic performances. Understanding of the deactivation mechanism and the type/morphology of the carbonaceous residues (whisker carbon versus active carbons) formed on the catalyst can significantly lead to a better catalyst design toward more stability. Future directions to design a potent catalyst for syngas production from methane could include the use of high surface area supports, such as metal organic frameworks (MOFs), which can act as excellent supports for high metal dispersions. Furthermore, a better understanding of the catalyst deactivation process using in situ catalytic experiments is significantly beneficial for the catalyst development purposes.

**Acknowledgments:** The authors gratefully acknowledge the financial support from the Faculty of Graduate Studies and Research (University of Regina), the Natural Sciences and Engineering Research Council of Canada (NSERC), the Canada Foundation for Innovation (CFI), and the Clean Energy Technologies Research Institute (CETRI).

**Author Contributions:** Hussameldin Ibrahim secured funding and proposed the original idea; Hussameldin Ibrahim and Amr Henni provided direction and guidance; Mohammed Mohamedali wrote the manuscript; Hussameldin Ibrahim and Amr Henni provided critical revision of the paper; Hussameldin Ibrahim supervised the project and provided final approval of the version to be published.

**Conflicts of Interest:** The authors declare no conflict of interest.

## References

1. Liu, K.; Song, C.; Subramani, V. *Hydrogen and Syngas Production and Purification Technologies*; John Wiley & Sons: Hoboken, NJ, USA, 2009.
2. Abatzoglou, N.; Fauteux-Lefebvre, C. Review of catalytic syngas production through steam or dry reforming and partial oxidation of studied liquid compounds. *Wiley Interdiscip. Rev. Energy Environ.* **2016**, *2*, 169–187. [[CrossRef](#)]
3. Wilhelm, D.J.; Simbeck, D.R.; Karp, A.D.; Dickenson, R.L. Syngas production for gas-to-liquids applications: Technologies, issues and outlook. *Fuel Process. Technol.* **2001**, *71*, 139–148. [[CrossRef](#)]
4. Rostrup-Nielsen, J.R. New aspects of syngas production and use. *Catal. Today* **2000**, *63*, 159–164. [[CrossRef](#)]
5. Abdullah, B.; Ghani, N.A.A.; Vo, D.-V.N. Recent advances in dry reforming of methane over Ni-based catalysts. *J. Clean. Prod.* **2017**, *162*, 170–185. [[CrossRef](#)]
6. Yusuf, R.O.; Noor, Z.Z.; Abba, A.H.; Hassan, M.A.A.; Din, M.F.M. Methane emission by sectors: A comprehensive review of emission sources and mitigation methods. *Renew. Sustain. Energy Rev.* **2012**, *16*, 5059–5070. [[CrossRef](#)]
7. Frontera, P.; Macario, A.; Aloise, A.; Antonucci, P.L.; Giordano, G.; Nagy, J.B. Effect of support surface on methane dry-reforming catalyst preparation. *Catal. Today* **2013**, *218*, 18–29. [[CrossRef](#)]

8. Mo, W.; Ma, F.; Liu, Y.; Liu, J.; Zhong, M.; Nulahong, A. Preparation of porous Al<sub>2</sub>O<sub>3</sub> by template method and its application in Ni-based catalyst for CH<sub>4</sub>/CO<sub>2</sub> reforming to produce syngas. *Int. J. Hydrogen Energy* **2015**, *40*, 16147–16158. [[CrossRef](#)]
9. Bang, S.; Hong, E.; Baek, S.W.; Shin, C.-H. Effect of acidity on Ni catalysts supported on P-modified Al<sub>2</sub>O<sub>3</sub> for dry reforming of methane. *Catal. Today* **2018**, *303*, 100–105. [[CrossRef](#)]
10. Das, S.; Sengupta, M.; Patel, J.; Bordoloi, A. A study of the synergy between support surface properties and catalyst deactivation for CO<sub>2</sub> reforming over supported Ni nanoparticles. *Appl. Catal. A Gen.* **2017**, *545*, 113–126. [[CrossRef](#)]
11. Zhang, R.-J.; Xia, G.-F.; Li, M.-F.; Wu, Y.; Nie, H.; Li, D.-D. Effect of support on the performance of Ni-based catalyst in methane dry reforming. *J. Fuel Chem. Technol.* **2015**, *43*, 1359–1365. [[CrossRef](#)]
12. Talkhoncheh, S.K.; Haghighi, M. Syngas production via dry reforming of methane over Ni-based nanocatalyst over various supports of clinoptilolite, ceria and alumina. *J. Nat. Gas Sci. Eng.* **2015**, *23*, 16–25. [[CrossRef](#)]
13. Wang, N.; Yu, X.; Shen, K.; Chu, W.; Qian, W. Synthesis, characterization and catalytic performance of MgO-coated Ni/SBA-15 catalysts for methane dry reforming to syngas and hydrogen. *Int. J. Hydrogen Energy* **2013**, *38*, 9718–9731. [[CrossRef](#)]
14. Akbari, E.; Alavi, S.M.; Rezaei, M. Synthesis gas production over highly active and stable nanostructured NiMgOAl<sub>2</sub>O<sub>3</sub> catalysts in dry reforming of methane: Effects of Ni contents. *Fuel* **2017**, *194*, 171–179. [[CrossRef](#)]
15. Titus, J.; Goepel, M.; Schunk, S.A.; Wilde, N.; Gläser, R. The role of acid/base properties in Ni/MgO-ZrO<sub>2</sub>-based catalysts for dry reforming of methane. *Catal. Commun.* **2017**, *100*, 76–80. [[CrossRef](#)]
16. Ay, H.; Üner, D. Dry reforming of methane over CeO<sub>2</sub> supported Ni, Co and Ni-Co catalysts. *Appl. Catal. B Environ.* **2015**, *179*, 128–138. [[CrossRef](#)]
17. Löfberg, A.; Guerrero-Caballero, J.; Kane, T.; Rubbens, A.; Jalowiecki-Duhamel, L. Ni/CeO<sub>2</sub> based catalysts as oxygen vectors for the chemical looping dry reforming of methane for syngas production. *Appl. Catal. B Environ.* **2017**, *212*, 159–174. [[CrossRef](#)]
18. Aghamohammadi, S.; Haghighi, M.; Maleki, M.; Rahemi, N. Sequential impregnation vs. sol-gel synthesized Ni/Al<sub>2</sub>O<sub>3</sub>-CeO<sub>2</sub> nanocatalyst for dry reforming of methane: Effect of synthesis method and support promotion. *Mol. Catal.* **2017**, *431*, 39–48. [[CrossRef](#)]
19. Han, J.; Zhan, Y.; Street, J.; To, F.; Yu, F. Natural gas reforming of carbon dioxide for syngas over Ni-Ce-Al catalysts. *Int. J. Hydrogen Energy* **2017**, *42*, 18364–18374. [[CrossRef](#)]
20. Taufiq-Yap, Y.H.; Sudarno; Rashid, U.; Zainal, Z. CeO<sub>2</sub>-SiO<sub>2</sub> supported nickel catalysts for dry reforming of methane toward syngas production. *Appl. Catal. A Gen.* **2013**, *468*, 359–369. [[CrossRef](#)]
21. Akbari, E.; Alavi, S.M.; Rezaei, M. CeO<sub>2</sub> Promoted Ni-MgO-Al<sub>2</sub>O<sub>3</sub> nanocatalysts for carbon dioxide reforming of methane. *J. CO<sub>2</sub> Util.* **2018**, *24*, 128–138. [[CrossRef](#)]
22. Muñoz, M.A.; Calvino, J.J.; Rodríguez-Izquierdo, J.M.; Blanco, G.; Arias, D.C.; Pérez-Omil, J.A.; Hernández-Garrido, J.C.; González-Leal, J.M.; Cauqui, M.A.; Yeste, M.P. Highly stable ceria-zirconia-yttria supported Ni catalysts for syngas production by CO<sub>2</sub> reforming of methane. *Appl. Surf. Sci.* **2017**, *426*, 864–873. [[CrossRef](#)]
23. Bao, Z.; Lu, Y.; Han, J.; Li, Y.; Yu, F. Highly active and stable Ni-based bimodal pore catalyst for dry reforming of methane. *Appl. Catal. A Gen.* **2015**, *491*, 116–126. [[CrossRef](#)]
24. Li, B.; Su, W.; Lin, X.; Wang, X. Catalytic performance and characterization of Neodymium-containing mesoporous silica supported nickel catalysts for methane reforming to syngas. *Int. J. Hydrogen Energy* **2017**, *42*, 12197–12209. [[CrossRef](#)]
25. Yabe, T.; Mitarai, K.; Oshima, K.; Ogo, S.; Sekine, Y. Low-temperature dry reforming of methane to produce syngas in an electric field over La-doped Ni/ZrO<sub>2</sub> catalysts. *Fuel Process. Technol.* **2017**, *158*, 96–103. [[CrossRef](#)]
26. Movasati, A.; Alavi, S.M.; Mazloom, G. CO<sub>2</sub> reforming of methane over Ni/ZnAl<sub>2</sub>O<sub>4</sub> catalysts: Influence of Ce addition on activity and stability. *Int. J. Hydrogen Energy* **2017**, *42*, 16436–16448. [[CrossRef](#)]
27. Mei, D.H.; Liu, S.Y.; Tu, X. CO<sub>2</sub> reforming with methane for syngas production using a dielectric barrier discharge plasma coupled with Ni/γ-Al<sub>2</sub>O<sub>3</sub> catalysts: Process optimization through response surface methodology. *J. CO<sub>2</sub> Util.* **2017**, *21*, 314–326. [[CrossRef](#)]

28. Meric, G.G.; Arbag, H.; Degirmenci, L. Coke minimization via SiC formation in dry reforming of methane conducted in the presence of Ni-based core-shell microsphere catalysts. *Int. J. Hydrogen Energy* **2017**, *42*, 16579–16588. [[CrossRef](#)]
29. Benrabaa, R.; Barama, A.; Boukhrouf, H.; Guerrero-Caballero, J.; Rubbens, A.; Bordes-Richard, E.; Löfberg, A.; Vannier, R.-N. Physico-chemical properties and syngas production via dry reforming of methane over NiAl<sub>2</sub>O<sub>4</sub> catalyst. *Int. J. Hydrogen Energy* **2017**, *42*, 12989–12996. [[CrossRef](#)]
30. Omoregbe, O.; Danh, H.T.; Nguyen-Huy, C.; Setiabudi, H.D.; Abidin, S.Z.; Truong, Q.D.; Vo, D.-V.N. Syngas production from methane dry reforming over Ni/SBA-15 catalyst: Effect of operating parameters. *Int. J. Hydrogen Energy* **2017**, *42*, 11283–11294. [[CrossRef](#)]
31. Albarazi, A.; Beaunier, P.; da Costa, P. Hydrogen and syngas production by methane dry reforming on SBA-15 supported nickel catalysts: On the effect of promotion by Ce<sub>0.75</sub>Zr<sub>0.25</sub>O<sub>2</sub> mixed oxide. *Int. J. Hydrogen Energy* **2013**, *38*, 127–139. [[CrossRef](#)]
32. Hossain, M.A.; Ayodele, B.V.; Cheng, C.K.; Khan, M.R. Artificial neural network modeling of hydrogen-rich syngas production from methane dry reforming over novel Ni/CaFe<sub>2</sub>O<sub>4</sub> catalysts. *Int. J. Hydrogen Energy* **2016**, *41*, 11119–11130. [[CrossRef](#)]
33. Wang, F.; Xu, L.; Shi, W. Syngas production from CO<sub>2</sub> reforming with methane over core-shell Ni@SiO<sub>2</sub> catalysts. *J. CO<sub>2</sub> Util.* **2016**, *16*, 318–327. [[CrossRef](#)]
34. Li, W.; Zhao, Z.; Jiao, Y. Dry reforming of methane towards CO-rich hydrogen production over robust supported Ni catalyst on hierarchically structured monoclinic zirconia nanosheets. *Int. J. Hydrogen Energy* **2016**, *41*, 17907–17921. [[CrossRef](#)]
35. Estephane, J.; Aouad, S.; Hany, S.; el Khoury, B.; Gennequin, C.; el Zakhem, H.; el Nakat, J.; Aboukaïs, A.; Aad, E.A. CO<sub>2</sub> reforming of methane over Ni-Co/ZSM5 catalysts. Aging and carbon deposition study. *Int. J. Hydrogen Energy* **2015**, *40*, 9201–9208. [[CrossRef](#)]
36. Albarazi, A.; Gálvez, M.E.; da Costa, P. Synthesis strategies of ceria-zirconia doped Ni/SBA-15 catalysts for methane dry reforming. *Catal. Commun.* **2015**, *59*, 108–112. [[CrossRef](#)]
37. Sharifi, M.; Haghighi, M.; Rahmani, F.; Karimipour, S. Syngas production via dry reforming of CH<sub>4</sub> over Co- and Cu-promoted Ni/Al<sub>2</sub>O<sub>3</sub>-ZrO<sub>2</sub> nanocatalysts synthesized via sequential impregnation and sol-gel methods. *J. Nat. Gas Sci. Eng.* **2014**, *21*, 993–1004. [[CrossRef](#)]
38. Mahoney, E.G.; Pusel, J.M.; Stagg-Williams, S.M.; Faraji, S. The effects of Pt addition to supported Ni catalysts on dry (CO<sub>2</sub>) reforming of methane to syngas. *J. CO<sub>2</sub> Util.* **2014**, *6*, 40–44. [[CrossRef](#)]
39. Abasaeed, A.E.; Al-Fatesh, A.S.; Naeem, M.A.; Ibrahim, A.A.; Fakeeha, A.H. Catalytic performance of CeO<sub>2</sub> and ZrO<sub>2</sub> supported Co catalysts for hydrogen production via dry reforming of methane. *Int. J. Hydrogen Energy* **2015**, *40*, 6818–6826. [[CrossRef](#)]
40. Ayodele, B.V.; Khan, M.R.; Cheng, C.K. Syngas production from CO<sub>2</sub> reforming of methane over ceria supported cobalt catalyst: Effects of reactants partial pressure. *J. Nat. Gas Sci. Eng.* **2015**, *27*, 1016–1023. [[CrossRef](#)]
41. Ayodele, B.V.; Khan, M.R.; Cheng, C.K. Catalytic performance of ceria-supported cobalt catalyst for CO-rich hydrogen production from dry reforming of methane. *Int. J. Hydrogen Energy* **2016**, *41*, 198–207. [[CrossRef](#)]
42. Ayodele, B.V.; Hossain, S.S.; Lam, S.S.; Osazuwa, O.U.; Khan, M.R.; Cheng, C.K. Syngas production from CO<sub>2</sub> reforming of methane over neodymium sesquioxide supported cobalt catalyst. *J. Nat. Gas Sci. Eng.* **2016**, *34*, 873–885. [[CrossRef](#)]
43. Ayodele, B.V.; Khan, M.R.; Lam, S.S.; Cheng, C.K. Production of CO-rich hydrogen from methane dry reforming over lanthania-supported cobalt catalyst: Kinetic and mechanistic studies. *Int. J. Hydrogen Energy* **2016**, *41*, 4603–4615. [[CrossRef](#)]
44. Mirzaei, F.; Rezaei, M.; Meshkani, F.; Fattah, Z. Carbon dioxide reforming of methane for syngas production over Co-MgO mixed oxide nanocatalysts. *J. Ind. Eng. Chem.* **2015**, *21*, 662–667. [[CrossRef](#)]
45. Zhang, G.; Zhao, P.; Xu, Y.; Qu, J. Characterization of Ca-promoted Co/AC catalyst for CO<sub>2</sub>-CH<sub>4</sub> reforming to syngas production. *J. CO<sub>2</sub> Util.* **2017**, *18*, 326–334. [[CrossRef](#)]
46. José-Alonso, D.S.; Illán-Gómez, M.J.; Román-Martínez, M.C. Low metal content Co and Ni alumina supported catalysts for the CO<sub>2</sub> reforming of methane. *Int. J. Hydrogen Energy* **2013**, *38*, 2230–2239. [[CrossRef](#)]
47. Wang, F.; Xu, L.; Zhang, J.; Zhao, Y.; Li, H.; Li, H.X.; Wu, K.; Xu, G.Q.; Chen, W. Tuning the metal-support interaction in catalysts for highly efficient methane dry reforming reaction. *Appl. Catal. B Environ.* **2016**, *180*, 511–520. [[CrossRef](#)]

48. Li, D.; Li, R.; Lu, M.; Lin, X.; Zhan, Y.; Jiang, L. Carbon dioxide reforming of methane over Ru catalysts supported on Mg-Al oxides: A highly dispersed and stable Ru/Mg(Al)O catalyst. *Appl. Catal. B Environ.* **2017**, *200*, 566–577. [[CrossRef](#)]
49. Cimino, S.; Lisi, L.; Mancino, G. Effect of phosphorous addition to Rh-supported catalysts for the dry reforming of methane. *Int. J. Hydrogen Energy* **2017**, *42*, 23587–23598. [[CrossRef](#)]
50. Kumar, S.; Kumar, B.; Kumar, S.; Jilani, S. Comparative modeling study of catalytic membrane reactor configurations for syngas production by CO<sub>2</sub> reforming of methane. *J. CO<sub>2</sub> Util.* **2017**, *20*, 336–346. [[CrossRef](#)]
51. De Vasconcelos, B.R.; Zhao, L.; Sharrock, P.; Nzihou, A.; Minh, D.P. Catalytic transformation of carbon dioxide and methane into syngas over ruthenium and platinum supported hydroxyapatites. *Appl. Surf. Sci.* **2016**, *390*, 141–156. [[CrossRef](#)]
52. Mohamedali, M.; Henni, A.; Ibrahim, H. *Hydrogen Production from Oxygenated Hydrocarbons: Review of Catalyst Development, Reaction Mechanism and Reactor Modeling*; Hydrogen Production Technologies; John Wiley & Sons, Inc.: Hoboken, NJ, USA, 2017; pp. 1–76.
53. You, X.; Wang, X.; Ma, Y.; Liu, J.; Liu, W.; Xu, X.; Peng, H.; Li, C.; Zhou, W.; Yuan, P.; et al. Ni-Co/Al<sub>2</sub>O<sub>3</sub> Bimetallic Catalysts for CH<sub>4</sub> Steam Reforming: Elucidating the Role of Co for Improving Coke Resistance. *ChemCatChem* **2014**, *6*, 3377–3386. [[CrossRef](#)]
54. Siang, T.J.; Singh, S.; Omoregbe, O.; Bach, L.G.; Phuc, N.H.H.; Vo, D.-V.N. Hydrogen production from CH<sub>4</sub> dry reforming over bimetallic Ni-Co/Al<sub>2</sub>O<sub>3</sub> catalyst. *J. Energy Inst.* **2017**, in press. [[CrossRef](#)]
55. Huo, J.; Jing, J.; Li, W. Reduction time effect on structure and performance of Ni-Co/MgO catalyst for carbon dioxide reforming of methane. *Int. J. Hydrogen Energy* **2014**, *39*, 21015–21023. [[CrossRef](#)]
56. Mahboob, S.; Haghghi, M.; Rahmani, F. Sonochemically preparation and characterization of bimetallic Ni-Co/Al<sub>2</sub>O<sub>3</sub>-ZrO<sub>2</sub> nanocatalyst: Effects of ultrasound irradiation time and power on catalytic properties and activity in dry reforming of CH<sub>4</sub>. *Ultrason. Sonochem.* **2017**, *38*, 38–49. [[CrossRef](#)] [[PubMed](#)]
57. Djinović, P.; Pintar, A. Stable and selective syngas production from dry CH<sub>4</sub>-CO<sub>2</sub> streams over supported bimetallic transition metal catalysts. *Appl. Catal. B Environ.* **2017**, *206*, 675–682. [[CrossRef](#)]
58. Xin, J.; Cui, H.; Cheng, Z.; Zhou, Z. Bimetallic Ni-Co/SBA-15 catalysts prepared by urea co-precipitation for dry reforming of methane. *Appl. Catal. A Gen.* **2018**, *554*, 95–104. [[CrossRef](#)]
59. Erdogan, B.; Arbag, H.; Yasyerli, N. SBA-15 supported mesoporous Ni and Co catalysts with high coke resistance for dry reforming of methane. *Int. J. Hydrogen Energy* **2018**, *43*, 1396–1405. [[CrossRef](#)]
60. Margossian, T.; Larmier, K.; Kim, S.M.; Krumeich, F.; Müller, C.; Copéret, C. Supported Bimetallic NiFe Nanoparticles through Colloid Synthesis for Improved Dry Reforming Performance. *ACS Catal.* **2017**, *7*, 6942–6948. [[CrossRef](#)]
61. Kim, S.M.; Abdala, P.M.; Margossian, T.; Hosseini, D.; Foppa, L.; Armutlulu, A.; van Beek, W.; Comas-Vives, A.; Copéret, C.; Müller, C. Cooperativity and Dynamics Increase the Performance of NiFe Dry Reforming Catalysts. *J. Am. Chem. Soc.* **2017**, *139*, 1937–1949. [[CrossRef](#)] [[PubMed](#)]
62. Paksoy, A.I.; Caglayan, B.S.; Aksoylu, A.E. A study on characterization and methane dry reforming performance of Co-Ce/ZrO<sub>2</sub> catalyst. *Appl. Catal. B Environ.* **2015**, *168*, 164–174. [[CrossRef](#)]
63. Sharifi, M.; Haghghi, M.; Abdollahifar, M. Sono-dispersion of bimetallic Ni-Co over zeolite Y used in conversion of greenhouse gases CH<sub>4</sub>/CO<sub>2</sub> to high valued syngas. *J. Nat. Gas Sci. Eng.* **2015**, *23*, 547–558. [[CrossRef](#)]
64. Khavarian, M.; Chai, S.-P.; Mohamed, A.R. The effects of process parameters on carbon dioxide reforming of methane over Co-Mo-MgO/MWCNTs nanocomposite catalysts. *Fuel* **2015**, *158*, 129–138. [[CrossRef](#)]
65. Aw, M.S.; Črnivec, I.G.O.; Pintar, A. Tunable ceria-zirconia support for nickel-cobalt catalyst in the enhancement of methane dry reforming with carbon dioxide. *Catal. Commun.* **2014**, *52*, 10–15. [[CrossRef](#)]
66. Rahemi, N.; Haghghi, M.; Babaluo, A.A.; Allahyari, S.; Jafari, M.F. Syngas production from reforming of greenhouse gases CH<sub>4</sub>/CO<sub>2</sub> over Ni-Cu/Al<sub>2</sub>O<sub>3</sub> nanocatalyst: Impregnated vs. plasma-treated catalyst. *Energy Convers. Manag.* **2014**, *84*, 50–59. [[CrossRef](#)]
67. Yao, L.; Zhu, J.; Peng, X.; Tong, D.; Hu, C. Comparative study on the promotion effect of Mn and Zr on the stability of Ni/SiO<sub>2</sub> catalyst for CO<sub>2</sub> reforming of methane. *Int. J. Hydrogen Energy* **2013**, *38*, 7268–7279. [[CrossRef](#)]
68. Fakeeha, A.H.; Naeem, M.A.; Khan, W.U.; Al-Fatesh, A.S. Syngas production via CO<sub>2</sub> reforming of methane using Co-Sr-Al catalyst. *J. Ind. Eng. Chem.* **2014**, *20*, 549–557. [[CrossRef](#)]
69. Sehested, J. Four challenges for nickel steam-reforming catalysts. *Catal. Today* **2006**, *111*, 103–110. [[CrossRef](#)]

70. Zhang, Y.; Wang, W.; Wang, Z.; Zhou, X.; Wang, Z.; Liu, C.-J. Steam reforming of methane over Ni/SiO<sub>2</sub> catalyst with enhanced coke resistance at low steam to methane ratio. *Catal. Today* **2015**, *256*, 130–136. [[CrossRef](#)]
71. Kho, E.T.; Scott, J.; Amal, R. Ni/TiO<sub>2</sub> for low temperature steam reforming of methane. *Chem. Eng. Sci.* **2016**, *140*, 161–170. [[CrossRef](#)]
72. Bej, B.; Pradhan, N.C.; Neogi, S. Production of hydrogen by steam reforming of methane over alumina supported nano-NiO/SiO<sub>2</sub> catalyst. *Catal. Today* **2013**, *207*, 28–35. [[CrossRef](#)]
73. Shinde, V.M.; Madras, G. Catalytic performance of highly dispersed Ni/TiO<sub>2</sub> for dry and steam reforming of methane. *RSC Adv.* **2014**, *4*, 4817–4826. [[CrossRef](#)]
74. Katheria, S.; Gupta, A.; Deo, G.; Kunzru, D. Effect of calcination temperature on stability and activity of Ni/MgAl<sub>2</sub>O<sub>4</sub> catalyst for steam reforming of methane at high pressure condition. *Int. J. Hydrogen Energy* **2016**, *41*, 14123–14132. [[CrossRef](#)]
75. Silveira, E.B.; Rabelo-Neto, R.C.; Noronha, F.B. Steam reforming of toluene, methane and mixtures over Ni/ZrO<sub>2</sub> catalysts. *Catal. Today* **2017**, *289*, 289–301. [[CrossRef](#)]
76. Lim, Z.-Y.; Wu, C.; Wang, W.G.; Choy, K.-L.; Yin, H. Porosity effect on ZrO<sub>2</sub> hollow shells and hydrothermal stability for catalytic steam reforming of methane. *J. Mater. Chem. A* **2016**, *4*, 153–159. [[CrossRef](#)]
77. Fang, X.; Zhang, X.; Guo, Y.; Chen, M.; Liu, W.; Xu, X.; Peng, H.; Gao, Z.; Wang, X.; Li, C. Highly active and stable Ni/Y<sub>2</sub>Zr<sub>2</sub>O<sub>7</sub> catalysts for methane steam reforming: On the nature and effective preparation method of the pyrochlore support. *Int. J. Hydrogen Energy* **2016**, *41*, 11141–11153. [[CrossRef](#)]
78. Zhang, J.; Zhang, T.; Zhang, X.; Liu, W.; Liu, H.; Qiu, J.; Yeung, K.L. New synthesis strategies for Ni/Al<sub>2</sub>O<sub>3</sub>-Sil-1 core-shell catalysts for steam reforming of methane. *Catal. Today* **2014**, *236*, 34–40. [[CrossRef](#)]
79. Andrade, M.L.; Almeida, L.; Rangel, M.D.C.; Pompeo, F.; Nichio, N. Ni-Catalysts Supported on Gd-Doped Ceria for Solid Oxide Fuel Cells in Methane Steam Reforming. *Chem. Eng. Technol.* **2014**, *37*, 343–348. [[CrossRef](#)]
80. Kim, N.Y.; Yang, E.-H.; Lim, S.-S.; Jung, J.S.; Lee, J.-S.; Hong, G.H.; Noh, Y.-S.; Lee, K.Y.; Moon, D.J. Hydrogen production by steam reforming of methane over mixed Ni/MgAl + CrFe<sub>3</sub>O<sub>4</sub> catalysts. *Int. J. Hydrogen Energy* **2015**, *40*, 11848–11854. [[CrossRef](#)]
81. Yang, X.; Da, J.; Yu, H.; Wang, H. Characterization and performance evaluation of Ni-based catalysts with Ce promoter for methane and hydrocarbons steam reforming process. *Fuel* **2016**, *179*, 353–361. [[CrossRef](#)]
82. Ali, S.; Al-Marri, M.J.; Abdelmoneim, A.G.; Kumar, A.; Khader, M.M. Catalytic evaluation of nickel nanoparticles in methane steam reforming. *Int. J. Hydrogen Energy* **2016**, *41*, 22876–22885. [[CrossRef](#)]
83. Mundhwa, M.; Thurgood, C.P. Methane steam reforming at low steam to carbon ratios over alumina and yttria-stabilized-zirconia supported nickel-spinel catalyst: Experimental study and optimization of microkinetic model. *Fuel Process. Technol.* **2017**, *168*, 27–39. [[CrossRef](#)]
84. Roy, P.S.; Park, C.S.; Raju, A.S.K.; Kim, K. Steam-biogas reforming over a metal-foam-coated (Pd-Rh)/(CeZrO<sub>2</sub>-Al<sub>2</sub>O<sub>3</sub>) catalyst compared with pellet type alumina-supported Ru and Ni catalysts. *J. CO<sub>2</sub> Util.* **2015**, *12*, 12–20. [[CrossRef](#)]
85. Jaiswar, V.K.; Katheria, S.; Deo, G.; Kunzru, D. Effect of Pt doping on activity and stability of Ni/MgAl<sub>2</sub>O<sub>4</sub> catalyst for steam reforming of methane at ambient and high pressure condition. *Int. J. Hydrogen Energy* **2017**, *42*, 18968–18976. [[CrossRef](#)]
86. Mei, D.; Glezakou, V.-A.; Lebarbier, V.; Kovarik, L.; Wan, H.; Albrecht, K.O.; Gerber, M.; Rousseau, R.; Dagle, R.A. Highly active and stable MgAl<sub>2</sub>O<sub>4</sub>-supported Rh and Ir catalysts for methane steam reforming: A combined experimental and theoretical study. *J. Catal.* **2014**, *316*, 11–23. [[CrossRef](#)]
87. De Castro, T.P.; Silveira, E.B.; Rabelo-Neto, R.C.; Borges, L.E.P.; Noronha, F.B. Study of the performance of Pt/Al<sub>2</sub>O<sub>3</sub> and Pt/CeO<sub>2</sub>/Al<sub>2</sub>O<sub>3</sub> catalysts for steam reforming of toluene, methane and mixtures. *Catal. Today* **2017**. [[CrossRef](#)]
88. Nieva, M.A.; Villaverde, M.M.; Monzón, A.; Garetto, T.F.; Marchi, A.J. Steam-methane reforming at low temperature on nickel-based catalysts. *Chem. Eng. J.* **2014**, *235*, 158–166. [[CrossRef](#)]
89. Arcotumapathy, V.; Vo, D.-V.N.; Chesterfield, D.; Tin, C.T.; Siahvashi, A.; Lucien, F.P.; Adesina, A.A. Catalyst design for methane steam reforming. *Appl. Catal. A Gen.* **2014**, *479*, 87–102. [[CrossRef](#)]
90. Rodemerck, U.; Schneider, M.; Linke, D. Improved stability of Ni/SiO<sub>2</sub> catalysts in CO<sub>2</sub> and steam reforming of methane by preparation via a polymer-assisted route. *Catal. Commun.* **2017**, *102*, 98–102. [[CrossRef](#)]

91. Duarte, R.B.; Krumeich, F.; van Bokhoven, J.A. Structure, Activity, and Stability of Atomically Dispersed Rh in Methane Steam Reforming. *ACS Catal.* **2014**, *4*, 1279–1286. [[CrossRef](#)]
92. Wu, H.; la Parola, V.; Pantaleo, G.; Puleo, F.; Venezia, A.; Liotta, L. Ni-Based Catalysts for Low Temperature Methane Steam Reforming: Recent Results on Ni-Au and Comparison with Other Bi-Metallic Systems. *Catalysts* **2013**, *3*, 563–583. [[CrossRef](#)]
93. Honsi, D.; Aouad, S.; Gennequin, C.; Aboukaïs, A.; Abi-Aad, E. A highly reactive and stable Ru/Co<sub>6-x</sub>Mg<sub>x</sub>Al<sub>2</sub> catalyst for hydrogen production via methane steam reforming. *Int. J. Hydrogen Energy* **2014**, *39*, 10101–10107. [[CrossRef](#)]
94. Wang, M.; Fu, Z.; Yang, Z. Tuning the Performance of Ni-Based Catalyst by Doping Coinage Metal on Steam Reforming of Methane and Carbon-Tolerance. *Fuel Cells* **2014**, *14*, 251–258. [[CrossRef](#)]



© 2018 by the authors. Licensee MDPI, Basel, Switzerland. This article is an open access article distributed under the terms and conditions of the Creative Commons Attribution (CC BY) license (<http://creativecommons.org/licenses/by/4.0/>).